1-1-2013

Photoacoustic Detection and Optical Spectroscopy of High-Intensity Focused Ultrasound-Induced Thermal Lesions in Biologic Tissue

Mosa Alhamami
Ryerson University

PHOTOACOUSTIC DETECION AND OPTICAL SPECTROSCOPY OF HIGH-INTENSITY FOCUSED ULTRASOUND-INDUCED THERMAL LESIONS IN BIOLOGIC TISSUE

by

Mosa Alhamami

B.Sc., Ryerson University, 2011

A thesis

presented to Ryerson University

in partial fulfillment of the

requirements for the degree of

Master of Science

in the Program of

Biomedical Physics

Toronto, Ontario, Canada, 2013

AUTHOR'S DECLARATION

I hereby declare that I am the sole author of this thesis. This is a true copy of the thesis, including any required final revisions, as accepted by my examiners.

I authorize Ryerson University to lend this thesis to other institutions or individuals for the purpose of scholarly research.

I further authorize Ryerson University to reproduce this thesis by photocopying or by other means, in total or in part, at the request of other institutions or individuals for the purpose of scholarly research.

I understand that my thesis may be made electronically available to the public.

ABSTRACT

Photoacoustic Detection and Optical Spectroscopy of High-Intensity Focused Ultrasound-Induced Thermal Lesions in Biologic Tissue

Mosa Alhamami

Master of Science, Biomedical Physics

Department of Physics, Ryerson University, 2013

In this study, the capability of a photoacoustic (PA) method in detecting high-intensity focused ultrasound (HIFU) thermal lesions was investigated in chicken breast tissue *in vitro* and the optical properties of the HIFU-treated and native tissues were determined. Created with a 1-MHz HIFU transducer, the detectability of the induced thermal lesions was assessed photoacoustically at 720 and 845 nm and their optical properties were characterized in the wavelength range 500-900 nm. The results show that the averaged ratio of the peak-to-peak PA signal amplitude of HIFU-treated tissue to that of native tissue is more than 3 fold. The optical spectroscopy investigation revealed that the absorption and reduced scattering coefficients are higher for HIFU-treated tissues than native tissues. This work demonstrates the capability of the PA method in detecting HIFU-induced thermal lesions due, in part, to the increase in their optical absorption coefficient, reduced scattering coefficient, and deposited laser energy fluence.

ACKNOWLEDMENTS

I would like to sincerely thank Dr. Jahan Tavakkoli for acting as my thesis supervisor. His thoughtful insights have been of utmost importance during this project. I am forever indebted to him for his continuous encouragement and endorsement to the many aspects of my professional career, including, but not limited to, advices and numerous reference letters. Thank you very, very much Dr. Tavakkoli for every minute of your time and for your timely feedback on my reports, abstracts, manuscript, thesis, etc. Thank you very much for giving me the opportunity to develop crucial research and critical thinking skills, pursue cutting-edge research and attend many scientific meetings/conferences. I have truly enjoyed my time working under your supervision since May 2010, when I was an undergraduate research assistant. I am indeed grateful to have had the opportunity to work with such a professional professor.

I would like to thank Drs. Michael Kolios and Alexandre Douplik for being in my supervisory committee. I have benefited from fruitful discussions with them. Dr. Kolios is gratefully acknowledged for also being in my thesis exam committee. I have indeed benefited from his expertise. Thank you very much, Dr. Kolios, for your feedback and comments on my thesis/manuscript. I would like also to thank Dr. Vladislav Toronov for acting as an external thesis examiner as well as Dr. Carl Kumaradas for chairing my thesis exam committee.

Thank you to all the faculty members, staff and students of the Departments of Physics for making my 6 years at Ryerson memorable. Specifically, I would like to highlight two colleagues from the Department of Physics for their invaluable help during this project: Eno Hysi for his help in the photoacoustic experiments and Martin Hohmann for his help in the optical spectroscopy measurements. I would also like to thank Pooya Sobhe Bidari, Yevgeniy Davletshin, Homa Assadi and Ashkan Bargriz Farshi for their help during some of the

experiments. Mojtaba Hajihasani is acknowledged for his help and ideas in using MATLAB for efficient data analysis and plotting of publication-quality figures. Special thanks extend to Arthur Worthington for his resourcefulness and technical support throughout this project.

Lastly but most importantly, I would like to thank my parents and my sisters for their continuous help and unconditional love. While he is not here anymore, my father has been a great source of encouragement since the day I was born till he died in 2010. My mother has been an amazing source of inspiration. Thank you very much, mom and dad, for your never-ending motivations towards achieving my dreams. Your words of love, support and encouragement ring in my ears whenever I think of you, lovely family. Thanks to my wonderful sister Mays Alhamami for her help with the schematic diagrams. I am truly blessed to have such a beautiful family.

This work was partially supported by the Ontario Research Fund- Research Excellence (ORF-RE) grant and the Natural Science and Engineering Research Council of Canada (NSERC Discovery grant) that were awarded to Dr. J. Tavakkoli.

This thesis is dedicated to my parents

TABLE OF CONTENTS

LIST OF SYMBOLS AND ABBREVIATIONS

$\Delta P(z)$ = Photoacoustic pressure rise

z = Depth

Γ = Grüneisen parameter

$E_{abs}(z)$ = Absorbed optical energy

μ_a= Optical absorption coefficient

$\Psi(z)$ = Laser energy fluence

c_s= Speed of sound

C_p= Heat capacity at constant pressure

β = Thermal coefficient of volume expansion

μ_{eff}= Effective optical attenuation coefficient

μ_s'= Reduced scattering coefficient

D_{eff}= Effective light penetration depth

I_{SPTA} = Spatial-peak, temporal-averaged intensity

SEM= Standard error of the mean

CCD = Charge-coupled device

L_T = Distance of ultrasound propagation in tissue

L_W = Distance of ultrasound propagation in water

F_L = Focal length of the HIFU transducer

LATS = Linear acoustic & temperature simulation

$L(\boldsymbol{r}, \hat{\boldsymbol{s}})$= Radiance at position $\boldsymbol{r}$ and in direction $\hat{\boldsymbol{s}}$

HIFU = High-intensity focused ultrasound

ROI = Regions of interest

US = Ultrasound

MR = Magnetic resonance

PA = Photoacoustic

EM = Electromagnetic

mK = Millikelvin

DR = Diffuse reflectance

TT = Total transmittance

RTE = Radiative transport equation

IAD = Inverse adding-doubling

RF = Radio-frequency

TD = Thermal dose

T(t) = Temperature as a function of time, t

n = Attenuation frequency dependency

M_R = Reflectance measurement

M_T = Transmittance measurement

μ_t= Total attenuation

$p(\hat{\boldsymbol{s}}, \widehat{\boldsymbol{s}'})$= Phase function

dw' = differential solid angle in direction $\widehat{\boldsymbol{s}'}$

LIST OF TABLES

LIST OF FIGURES

LIST OF APPENDICES

Chapter 1: Introduction

1.1 Therapeutic ultrasound

The use of medical ultrasound in therapy predates its use in imaging. In 1927, Wood and Loomis found (as cited in Ref. [1]) that high-intensity ultrasound can produce therapeutic effects in biologic systems. The work of Wood and Loomis opened the doors for subsequent research and development in therapeutic ultrasound, which initially focused on the thermally-induced therapeutic benefits of ultrasound by utilizing the acoustic absorption of propagating waves.[1] However, non-thermal ultrasound applications started to arise afterward,[1] expanding the potential applicability of ultrasound in medicine and biology. The increased interest in using ultrasound for therapeutic purposes can primarily be attributed to its portability, cost-effectiveness, ease-of-use, and non-invasiveness. Moreover, therapeutic ultrasound utilizes non-ionizing radiation, making it an attractive alternative in many applications, including cancer treatment.

The advantages of ultrasound have been exploited to develop various applications in biomedicine. Currently, there are several ultrasound therapies, each of which has its own application(s). These therapies have been classified based on the delivered acoustic energy into low-power and high-power ultrasound therapies.[1] Low-power ultrasound therapies include sonoporation, sonophoresis, sonothrombolysis, gene therapy, and bone and wound healing; on the other hand, high-power ultrasound therapies include physiotherapy, lithotripsy, histotripsy, and high-intensity focused ultrasound (HIFU).[1, 2] Table 1-1 provides a brief description of each one of the aforementioned ultrasound therapies.

Table 1-1: A summary of the main ultrasound therapies

Low-power ultrasound therapies	**High-power ultrasound therapies**
Sonoporation: the application of ultrasound for transient alteration of cellular membrane structure, allowing increased uptake of molecules of interest into the cell.[1]	*Physiotherapy:* the application of ultrasound in softening scar tissue, the resolution of edema, and the treatment of soft tissue injuries, among other applications.[1]
Sonophoresis: the application of ultrasound to enhance the penetration of drugs through the skin layers.[1]	*Lithotripsy:* the application of ultrasound to disintegrate gallbladder and kidney stones using shock waves.[3]
Sonothrombolysis: the application of ultrasound, on its own or combined with a drug/contrast agent, in the dissolution of blood clots.[1]	*Histotripsy:* the application of ultrasound for cellular destruction through mechanical fragmentation and subdivision of biological tissues.[4]
Gene therapy: the application of ultrasound to facilitate the delivery of genes into cells.[1]	*HIFU:* application of ultrasound to selectively coagulate regions of interest (ROI) in biologic tissues through the formation of thermal lesions by a focalized beam. The localized deposition of acoustic energy within the ROI results in rapid temperature rise and subsequent coagulation, while sparing intervening tissues.[5]
Bone and wound healing: the application of ultrasound to accelerate bone fracture healing by inducing direct ossification,[1] and the application of ultrasound to accelerate wound healing.[6]	

1.2 High-intensity focused ultrasound (HIFU)

1.2.1 HIFU therapeutic mechanisms

The hallmark of HIFU therapy is its capability of inducing therapeutic benefits in deep-seated ROIs in tissue selectively and non-invasively.[7] Such therapeutic benefits can be achieved by the high acoustic power and the strong focusing of the therapeutic transducer, resulting in localized deposition of intensive acoustic energy within the transducer's focal zone.[7] The deposition of acoustic energy results in a very rapid elevation in the tissue temperature within the focal zone of the HIFU transducer, while sparing intervening tissue layers. The *thermal* and *mechanical* mechanisms of HIFU therapy, described below, play an important role in its induced biologic effects in tissues.[7] These mechanisms can result in protein denaturation and immediate cell death when the temperature of the targeted tissue exceeds 56 ^{o}C for at least 1 second of sonication time,[8] in a process known as coagulation necrosis.[7] Because the temperature of the targeted tissue undergoes a rapid and localized increase, the cytotoxicity is confined in space and the coagulated tissue volume (as known as thermal lesion) is focalized and trackless, with no surrounding tissue damage.[5] This feature distinguishes HIFU from other ablative treatments, such as laser and radiofrequency thermal therapies, that require the introduction of an applicator into the ROI.[5]

1.2.1.1 Thermal mechanism of HIFU

The propagation of an ultrasound beam through biologic tissues results in an exponential attenuation of its acoustic pressure amplitude and intensity.[9] Although both acoustic scattering and absorption take place,[9] the dominant loss mechanism is acoustic absorption,[10] which results in temperature rise and tissue heating.[11] When the temperature rise and the ultrasound exposure duration are sufficient enough, an irreversible thermal tissue damage can be induced in biologic

tissues.[9, 11] The amount of tissue damage can be determined when both the exposure duration and the achieved temperature are combined using a concept known as thermal dose (*TD*),[11] which is given by the following mathematical expression[12]:

$$TD = \int_{t1}^{t2} R^{43-T(t)}\, dt \qquad (1\text{-}1)$$

where *R* is a constant and equals to 0.5 for temperatures above 43.0 ^{o}C and 0.25 for temperatures below 43.0 ^{o}C. Here, *t1* and *t2* are the initial and final times, respectively, and *T (t)* is the temperature, in ^{o}C, as a function of time, *t*.[12]

1.2.1.2 Mechanical mechanism of HIFU

The mechanical mechanism of HIFU therapy is manifested through several physical phenomena that can result in a range of biologic effects with therapeutic benefits. Among these phenomena are acoustic cavitation and radiation force.[13]

Acoustic cavitation occurs when ultrasound waves stimulate the formation of gas bubbles in the propagation medium as a result of subjecting localized regions to alternating increase and decrease in pressure amplitudes.[9] The gas bubbles exhibit dynamic behaviour, and can either be in a stable or a transient (inertial) cavitation sates.[9] In stable cavitation, the gas bubbles oscillate, contract, and expand without bursting.[14] On the other hand, in transient cavitation, the gas bubbles can completely collapse following large changes in size over a few acoustic cycles.[9] The collapse of gas bubbles in transient cavitation results in highly-localized, destructive effects that can induce the generation of shock (pressure) waves and can cause a local temperature rise.[14] While they do not produce such violent effects, the gas bubbles in stable cavitation also contribute to the therapeutic effect of HIFU by increasing acoustic reflections within a cavitating

region, thereby enhancing acoustic absorption, acoustic energy trapping, and the subsequent conversion of acoustic energy into heat within the cavitating region.[5]

Another physical phenomenon that occurs within the acoustic field of HIFU is radiation force. It is a result of applying acoustic pressure by propagating ultrasound waves on an object with a density that is different from that of the surrounding medium within the acoustic field.[9] Radiation force results in two types of motions on the targeted object: translational and rotational motions.[9] Within a localized area and at high incident acoustic intensities, the rotational motion can cause a rapid fluid movement, a phenomenon known as acoustic microstreaming. Biologic effects, such as macromolecule (e.g. protein) fragmentation, can be induced by acoustic microstreaming, thereby further enhancing the therapeutic benefits of HIFU.[9]

1.2.2 Image-guided HIFU

Research efforts to utilize the therapeutic benefits of HIFU have led to the development of HIFU systems for various applications in biomedicine. The successful application of these therapeutic systems, however, would not have been possible had it not been to the emergence of enabling technologies, such as diagnostic imaging devices. The use of imaging devices alongside with HIFU therapy was intended to provide a real-time monitoring, assessment and control of HIFU treatments, thereby improving the safety and efficacy of HIFU treatment as a potential bloodless surgery. Currently, most HIFU treatments are monitored and guided with magnetic resonance (MR) imaging and ultrasound (US) imaging. Because of their safety and use of non-ionizing radiation, the use of MR and US imaging modalities to guide HIFU treatments has been widely investigated.[15, 16] Image-guided HIFU has shown a great potential for various therapeutic

applications, including oncologic applications, such as treatments of prostate tumour,[17] uterine fibroids,[18] and breast fibroadenoma.[19]

1.2.3 Limitation of current HIFU imaging modalities

Despite its successful use in various applications, MR and US image-guided HIFU still pose some challenges. The challenges associated with MR image-guided HIFU include high equipment cost,[20] complexity and duration of the scans,[20] compatibility with the HIFU transducer,[21] and patient-access restrictions.[21] Moreover, the use of MR imaging with claustrophobic patients as well as patients with implanted pacemakers, aneurysm clips and prostheses is an issue.[20] The challenges associated with US imaging, on the other hand, include low contrast-resolution, sensitivity, and specificity[21] for the detection and monitoring of HIFU treatments in biologic tissues. Moreover, because the detection of HIFU treatments using conventional B-mode US imaging is heavily dependent on the appearance of hyperechoic spots at the HIFU focus,[22] B-mode US imaging would be incapable of visualizing HIFU treatments when HIFU-induced gas/vapor bubbles, which are responsible for the appearance of the hyperechoic spots,[22] are not produced in enough quantities.

1.3 Photoacoustics and its potential in thermal therapy

1.3.1 Principles of photoacoustics

The photoacoustic (PA) effect, which was first reported in 1880 by Alexander Graham Bell,[23] constitutes the basic physical principle behind PA imaging.[24] In the PA effect, the following processes take place[24, 25]: (a) the absorption of electromagnetic (EM) radiation by an object; (b) the conversion of the absorbed EM energy into heat, thereby raising the temperature

of the object slightly; (c) thermal expansion of the object as a result of the slight temperature rise, which is typically in the millikelvin (mK) range; and (d) the generation of acoustic waves in the medium. In PA imaging, the EM radiation is within the optical region (i.e. from visible to near infra-red), and the generated acoustic waves are wide-band ultrasound waves detectable by an ultrasound transducer.[26]

The laser-induced PA pressure rise, $\Delta P(z)$, in PA imaging is directly proportional to the absorbed optical energy and the thermo-acoustic efficiency, and is given by the following equation, [27, 28] assuming a plane-wave propagation in a homogenous medium[26]:

$$\Delta P(z) = \Gamma\, E_{abs}(z) \;=\; \Gamma\, \mu_a \Psi(z) \tag{1-2}$$

where $E_{abs}(z)$ [J/m^3] is the absorbed optical energy density from a laser source at depth z, and it is the product of the optical absorption coefficient, μ_a [m^{-1}], and the laser energy fluence, $\Psi(z)$ [J/m^2].[27] The symbol Γ denotes the dimensionless Grüneisen parameter. It is proportional to the fraction of thermal energy that is converted into acoustic waves[29] (also known as thermo-acoustic efficiency). The temperature-dependent Grüneisen parameter is given by the following equation[29]:

$$\Gamma = \frac{\beta\, c_s^2}{C_p} \tag{1-3}$$

where c_s [m/s] is the speed of sound in the medium; C_p[J/gK] is the heat capacity at a constant pressure; and β [K^{-1}] is the medium's thermal coefficient of volume expansion.[29]

It is important to note that the z-axial distribution of the PA pressure rise, $\Delta P(z)$, given in Eq. (1-2) is valid only when the laser-induced heating process is faster than the expansion of the medium.[29] Additionally, in order to generate acoustic waves from the absorbing medium, the

heating source (i.e. the optical irradiation) must be time variant, since a steady thermal expansion, which is time invariant, does not result in the production of acoustic waves.[25, 30]

1.3.2 The potential of PA detection of HIFU treatments

As an alternative to MR and US imaging modalities, PA imaging was proposed to provide assessment and guidance of HIFU treatments. Previous research efforts have successfully utilized PA imaging to detect HIFU-induced thermal lesions *in vitro*,[31, 21] *ex vivo*,[32] and *in vivo*.[33] In some *in vitro* and *ex vivo* studies[21, 32] of PA detection of HIFU-induced thermal lesions, an increase in the PA signal amplitude was observed. On the other hand, Chitnis et al.[33] observed a decrease in the PA signal of HIFU-treated tissue in their *in vivo* study. The discrepancy between the *in vitro/ex vivo* and *in vivo* results can be primarily attributed to the different HIFU-induced thermochemical reactions in live tissues compared to excised tissues due to blood perfusion being significantly different in the two cases.[33] In their *in vitro* investigation, Khokhlova et al.[31] have attributed the PA contrast between HIFU-treated and native tissues to the thermally-induced formation of methemoglobin,[31] which results in an enhancement in the optical absorption coefficient.[34, 35] Moreover, Khokhlova et al.[31] have also attributed the PA contrast between HIFU-treated and native tissues to tissue dehydration, which results in an increase in the concentration of absorbing and scattering centres.[31, 36] On the other hand, the decrease in the PA signal after HIFU-induced coagulation *in vivo* has been attributed to the reduction of blood content in the HIFU-treated tissue volume and the breakage of chemical bonds that are responsible for light absorption in the near infra-red region, thereby reducing the tissue optical absorption.[33]

As for its advantages as a potential diagnostic technique in HIFU treatments, PA imaging combines the benefits of both ultrasound and optical imaging modalities, i.e. it provides higher resolution than optical imaging and higher tissue contrast than ultrasound imaging.[24] Moreover, the use of PA image-guided HIFU has been shown to enhance HIFU heating and temperature rise in real-time monitoring applications due to the PA laser-induced formation of cavitational bubbles,[37] which, as discussed earlier, enhance acoustic absorption and the subsequent conversion of acoustic energy into heat. Another advantage of PA imaging is that, unlike X-ray-based imaging modalities, it utilizes a non-ionizing EM radiation.

1.4 Optical spectroscopy of biologic tissues

In general, spectroscopy refers to the study of the interactions of EM waves with matter.[38] Tissue optical spectroscopy, in particular, refers to the study of the interactions of light (ranging from the ultraviolet to the infrared region) with biologic tissues through measurements of the wavelength-dependent tissue response to light in the form of optical spectra.[38] The tissue response to light, which may include transmission, reflection, absorption and scattering, can be measured with various techniques in order to obtain useful information about the tissue under examination.[38] In the context of this study, two of these techniques will be discussed for their importance in determining the optical absorption and reduced scattering coefficients of biologic tissues.[39] The techniques are: diffuse reflectance (DR) and total transmittance (TT) measurements, which were performed in this study using an integrating sphere attachment of a commercially-available spectrophotometer. DR measurements were performed by first sandwiching a tissue sample between two optical glass slides and placing it in the sample exit port of a measurement sphere (see Fig. 5, chapter 2). The reflected light from the tissue sample

was detected inside the measurement sphere. On the other hand, TT measurements were performed by placing the sandwiched tissue sample at the entrance port of the measurement sphere, while placing a standard barium sulfate-coated light reflector at the exit port of the measurement sphere (see Fig. 6, chapter 2). The transmitted light from the sandwiched tissue sample was detected inside the measurement sphere. In both the DR and TT measurements, the barium sulfate-coated wall of the measurement sphere acted as a reflector and, therefore, concentrated light into the sphere's detector.[40] It is important to note that prior to performing DR and TT measurements, a baseline measurement was performed, as depicted in Fig. 1-1.

It is noteworthy to mention that, in tissue optics, transmittance and reflectance, which are unitless quantities, refer to the light intensity being transmitted and reflected, respectively, by tissue, normalized by the incident light.[39]

In order to predict the distribution and the behaviour of light in a target medium, it is necessary to characterize the optical properties of that medium.[41] In biomedicine, optical property characterization is particularly important in the development of laser-based diagnostic and therapeutic modalities.[41] For instance, to study the feasibility of PA imaging to detect a blood vessel inside a tissue, knowledge about the absorption spectrum of the blood would be beneficial in order to optimize the detected PA signal[26] by using laser illumination wavelength that produces the maximum optical absorption in blood. Similarly, to study the effects of particular tissue treatments, such as HIFU treatments, on the detected PA signal amplitudes, knowledge about the absorption and scattering spectra of native and coagulated tissues would be beneficial. One method to characterize the optical properties of biologic tissues is to input the measured spectra of the optical spectroscopy experiments (DR and TT) in a simulation program

that solves the radiative transport equation (RTE), an analytical model of photon propagation,[38] to determine the optical absorption and reduced scattering coefficients.

One of the widely used methods to determine the optical properties, in conjunction with spectroscopic measurements, is the inverse adding-doubling (IAD) method.[42] In the IAD program,[43] which is available online, optical parameters such as scattering, absorption, and scattering anisotropy can be determined by repeatedly solving the RTE until a match with the measured reflection and transmission values is determined.[42] The "inverse" implies a reversal to the regular extraction of transmission and reflection values from the optical properties, whereas "adding-doubling" refers to the utilized methodology in solving the RTE.[42] The IAD method, therefore, converts the integrating-sphere measurements of DR and TT into optical absorption and reduced scattering coefficients.[39] It is a versatile method, and is well-suited to measurements employing biologic tissue specimens sandwiched between optical glass slides/plates.[42]

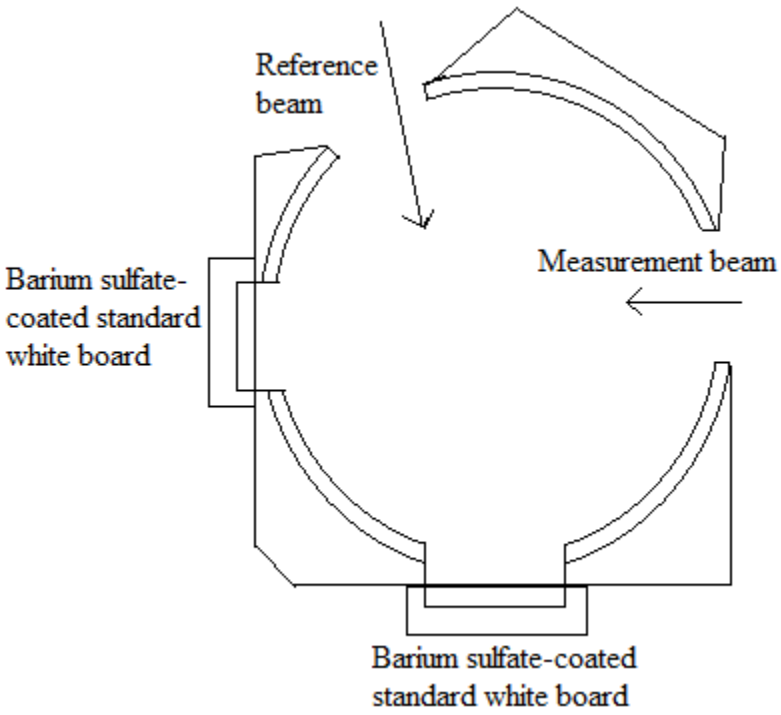

FIG. 1-1: A diagram of the baseline measurement performed in the integrating-sphere experiments (reproduced, with permission, from Ref.[40]; courtesy of Shimadzu Corporation).

1.5 Thesis hypothesis and specific aims

Based on previous works, the hypothesis of this study is that PA detection of HIFU-induced thermal lesions is feasible due, in part, to changes in the optical properties of HIFU-treated tissues. In order to test the hypothesis, the following specific aims have been set:

a) Demonstrating the possibility of PA detection of HIFU-induced thermal lesions in chicken breast tissues *in vitro* at two optical wavelengths (720 nm and 845 nm);
b) Determining the optical properties (total transmittance, diffuse reflectance, absorption coefficient, reduced scattering coefficient, effective attenuation coefficient, and light penetration depth) of HIFU-induced thermal lesions and comparing them with those of native (untreated) tissues in the wavelength range of 500-900 nm.

Chapter 1 bibliography

[1] G. ter Haar, "Therapeutic applications of ultrasound," Progress in Biophysics and Molecular Biology **93**, 111–129 (2007).

[2] S. Bhadane, High Intensity Focused Ultrasound and Microbubble Induced Tissue Ablation: Effect of Treatment Parameters on Thermal Lesion Volume and Temperature (Ryerson University, 2012).

[3] W. Sass, M. Bräunlich, H. Dreyer, E. Matura, W. Folberth, H. Priesmeyer, and J. Seifert, "The mechanisms of stone disintegration by shock waves," Ultrasound in Medicine & Biology **17**, 239–243 (1991).

[4] W.W. Roberts, T.L. Hall, K. Ives, J.S. Wolf, J.B. Fowlkes, and C.A. Cain, "Pulsed cavitational ultrasound: a noninvasive technology for controlled tissue ablation (histotripsy) in the rabbit kidney," The Journal of Urology **175**, 734–738 (2006).

[5] G. ter Haar and C. Coussios, "High intensity focused ultrasound: physical principles and devices," International Journal of Hyperthermia **23**, 89–104 (2007).

[6] H. Ikai, T. Tamura, T. Watanabe, M. Itou, A. Sugaya, S. Iwabuchi, Y. Mikuni-Takagaki, and S. Deguchi, "Low-intensity pulsed ultrasound accelerates periodontal wound healing after flap surgery," Journal of Periodontal Research **43**, 212–216 (2008).

[7] S. Vaezy, M. Andrew, P. Kaczkowski, and L. Crum, "Image-guided acoustic therapy," Annual Review of Biomedical Engineering **3**, 375–390 (2001).

[8] C.R. Hill and G.R. ter Haar, "High intensity focused ultrasound -- potential for cancer treatment," British Journal of Radiology **68**, 1296–1303 (1995).

[9] W. Hedrick, D. Hykes, and D. Starchman, *Ultrasound physics and instrumentation* (Elsevier Mosby, St. Louis, MO, 2004).

[10] J. Prince and J. Links, *Medical imaging signals and systems* (Pearson Prentice Hall, Upper Saddle River, NJ, 2006).

[11] G. ter Haar, "Ultrasound bioeffects and safety," Proceedings of the Institution of Mechanical Engineers, Part H: Journal of Engineering in Medicine **224**, 363–373 (2010).

[12] S. Sapareto and W. Dewey, "Thermal dose determination in cancer therapy," International Journal of Radiation Oncology Biology Physics **10**, 787–800 (1984).

[13] J.L. Foley, S. Vaezy, and L.A. Crum, "Applications of high-intensity focused ultrasound in medicine : Spotlight on neurological applications," Applied Acoustics **68**, 245–259 (2007).

[14] S.K. Edelman, *Understanding ultrasound physics* (ESP, Inc., Woodlands, TX, 2007).

[15] J. Tavakkoli and N.T. Sanghvi, "Ultrasound-guided HIFU and thermal ablation," in *Therapeutic Ultrasound: Mechanisms to Applications*, edited by V. Frenkel (Nova Science Publishers, Hauppauge, NY, 2011), pp. 137–161.

[16] K. Hynynen, "MRI-guided focused ultrasound treatments.," Ultrasonics **50**, 221–229 (2010).

[17] W.A. N'djin, M. Burtnyk, I. Kobelevskiy, S. Hadjis, M. Bronskill, and R. Chopra, "Coagulation of human prostate volumes with MRI-controlled transurethral ultrasound therapy: results in gel phantoms," Medical Physics **39**, 4524–4536 (2012).

[18] C.M.C. Tempany, E.A. Stewart, N. McDannold, B.J. Quade, F.A. Jolesz, and K. Hynynen, "MR imaging-guided focused ultrasound surgery of uterine leiomyomas: a feasibility study," Radiology **226**, 897–905 (2003).

[19] K. Hynynen, O. Pomeroy, D.N. Smith, P.E. Huber, N.J. McDannold, J. Kettenbach, J. Baum, S. Singer, and F.A. Jolesz, "MR imaging-guided focused ultrasound surgery of fibroadenomas in the breast: a feasibility study," Radiology **219**, 176–185 (2001).

[20] J. Bushberg, J. Seibert, E. LeidholdT, and J. Boone, *The essential physics of medical imaging*, 2nd ed. (Lippincott Williams & Wilkins, Philadelphia, PA, 2002).

[21] H. Cui and X. Yang, "Real-time monitoring of high-intensity focused ultrasound ablations with photoacoustic technique: an in vitro study," Medical Physics **38**, 5345–5350 (2011).

[22] S. Vaezy, X. Shi, R. Martin, E. Chi, P. Nelson, M. Bailey, and L. Crum, "Real-time visualization of high-intensity focused ultrasound treatment using ultrasound imaging," Ultrasound in Medicine & Biology **27**, 33–42 (2001).

[23] A.G. Bell, "On the production and reproduction of sound by light," American Journal of Sciences **20**, 305–324 (1880).

[24] M. Xu and L. V Wang, "Photoacoustic imaging in biomedicine," Review of Scientific Instruments **77**, 041101 (2006).

[25] C. Li and L. V Wang, "Photoacoustic tomography and sensing in biomedicine," Physics in Medicine and Biology **54**, R59 – R97 (2009).

[26] S. Mallidi, G.P. Luke, and S. Emelianov, "Photoacoustic imaging in cancer detection, diagnosis, and treatment guidance," Trends in Biotechnology **29**, 213–221 (2011).

[27] A.A. Oraevsky, S.L. Jacques, and F.K. Tittel, "Determination of tissue optical properties by piezoelectric detection of laser-induced stress waves," in *Laser-Tissue Interaction IV*, edited by S.L. Jacques and A. Katzir (Proc. SPIE 1882, 86-101, 1993).

[28] V.E. Gusev and A.A. Karabutov, *Laser Optoacoustics* (American Institute of Physics, New York, 1992).

[29] A.A. Oraevsky, S.L. Jacques, and F.K. Tittel, "Measurement of tissue optical properties by time-resolved detection of laser-induced transient stress," Applied Optics **36**, 402–415 (1997).

[30] E. Hysi, Photoacoustic Detection of Red Blood Cell Aggregation (Ryerson University, 2012).

[31] T. Khokhlova, I.M. Pelivanov, O.A. Sapozhnikov, V.S. Solomatin, and A.A. Karabutov, "Opto-acoustic diagnostics of the thermal action of high-intensity focused ultrasound on biological tissues: the possibility of its applications and model experiments," Quantum Electronics **36**, 1097–1102 (2006).

[32] Y. Sun and B.O. Neill, "Imaging high-intensity focused ultrasound-induced tissue denaturation by multispectral photoacoustic method: an ex vivo study," Applied Optics **52**, 1764–1770 (2013).

[33] P. Chitnis, H. Brecht, R. Su, and A. Oraevsky, "Feasibility of optoacoustic visualization of high-intensity focused ultrasound-induced thermal lesions in live tissue," Journal of Biomedical Optics **15**, 021313 (2010).

[34] J.F. Black and J.K. Barton, "Chemical and structural changes in blood undergoing laser photocoagulation.," Photochemistry and photobiology **80**, 89–97 (2004).

[35] J. Barton, G. Frangineas, H. Pummer, and J. Black, "Cooperative phenomena in two-pulse, two-color laser photocoagulation of cutaneous blood vessels," Photochemistry & Photobiology **73**, 642–650 (2001).

[36] A. Yaroslavsky, P. Schulze, I. Yaroslavsky, R. Schober, F. Ulrich, and H.-J. Schwarzmaier, "Optical properties of selected native and coagulated human brain tissues in vitro in the visible and near infrared spectral range," Physics in Medicine & Biology **47**, 2059–2073 (2002).

[37] H. Cui and X. Yang, "Enhanced-heating effect during photoacoustic imaging-guided high-intensity focused ultrasound," Applied Physics Letters **99**, 231113 (2011).

[38] A. Welch and M. van Gemert (eds.), *Optical-thermal response of laser-irradiated tissue*, 2nd ed. (Springer, New York, 2011).

[39] S. Prahl, "Everything I think you should know about inverse adding-doubling," Oregon Medical Laser Center, St. Vincent Hospital 1–74 (2011).

[40] Shimadzu Corporation, *Diffuse reflectance measurement*, (2013).

[41] K. Ishii, A. Kimura, and K. Awazu, "Optical properties of tissues after laser treatments in the wavelength range of 350 - 1000 nm," Proc. SPIE **6991**, 69912F (2008).

[42] S.A. Prahl, M.J.C. van Gemert, and A.J. Welch, "Determining the optical properties of turbid media by using the adding-doubling method," Applied Optics **32**, 559–568 (1993).

[43] S.A. Prahl, *Inverse Adding-Doubling program: Version 3-9-6*, (2013). (http://omlc.ogi.edu/software/iad/index.html)

Chapter 2: Photoacoustic detection and optical spectroscopy of high-intensity focused ultrasound-induced thermal lesions in biologic tissue

This chapter is a manuscript that was submitted to Medical Physics, an official science journal of the American Association of Physicists in Medicine (AAPM) and the Canadian Organization of Medical Physicists (COMP)/Canadian College of Physicists in Medicine (CCPM)/International Organization for Medical Physics (IOMP).

Manuscript#: 13-1365

Submission date: Sept. 6, 2013

M. Alhamami, M. Kolios, and J. Tavakkoli, "Photoacoustic detection and optical spectroscopy of high-intensity focused ultrasound-induced thermal lesions in biologic tissue," Medical Physics (submitted on Sept. 6, 2013).

Photoacoustic detection and optical spectroscopy of high-intensity focused ultrasound-induced thermal lesions in biologic tissue

Mosa Alhamami, Michael C. Kolios, and Jahan Tavakkoli[a)]

Department of Physics, Ryerson University, 350 Victoria Street, Toronto, ON, M5B 2K3 Canada

[a)] Electronic mail: jtavakkoli@ryerson.ca

Purpose: The aims of this study are: (a) to investigate the capability of photoacoustic (PA) method in detecting high-intensity focused ultrasound (HIFU) treatments in muscle tissues *in vitro*; and (b) to determine the optical properties of HIFU-treated and native tissues in order to assist in the interpretation of the observed contrast in PA detection of HIFU treatments.

Methods: A single-element, spherically-concaved HIFU transducer with a centre frequency of 1 MHz was utilized to create thermal lesions in chicken breast tissues *in vitro*. To investigate the detectability of HIFU treatments photoacoustically, PA detection was performed at 720 nm and 845 nm on 7 HIFU-treated tissue samples. Within each tissue sample, PA signals were acquired from 22 locations equally divided between two regions of interest within two volumes in tissue – a HIFU-treated volume and an untreated volume. Optical spectroscopy was then carried out on 10 HIFU-treated chicken breast specimens in the wavelength range of 500-900 nm, in 1-nm increments, using a spectrophotometer with an integrating sphere attachment. Our optical spectroscopy raw data (total transmittance and diffuse reflectance) were used to obtain the optical absorption and reduced scattering coefficients of HIFU-induced thermal lesions and native tissues by employing the inverse adding-doubling method. The aforementioned interaction coefficients were subsequently used to calculate the effective attenuation coefficient and light penetration depth of HIFU-treated and native tissues in the wavelength range of 500-900 nm.

Results: HIFU-treated tissues produced greater PA signals than native tissues at 720 and 845 nm. At 720 nm, the averaged ratio of the peak-to-peak PA signal amplitude of HIFU-treated tissue to that of native tissue was 3.68 ± 0.25 (mean ± standard error of the mean). At 845 nm, the averaged ratio of the peak-to-peak PA signal amplitude of HIFU-treated tissue to that of native tissue was 3.75 ± 0.26 (mean ± standard error of the mean). Our spectroscopic investigation has shown that HIFU-treated tissues have a greater optical absorption and reduced scattering coefficients than native tissues in the wavelength range of 500-900 nm. In fact, at 720 nm and 845 nm, the ratio of the optical absorption coefficient of HIFU-treated tissues to that of native tissues was 1.13 and 1.17, respectively; on the other hand, the ratio of the reduced scattering coefficient of HIFU-treated tissues to that of native tissues was 13.22 and 14.67 at 720 nm and 845 nm, respectively. Consequently, HIFU-treated tissues have a higher effective attenuation coefficient and a lower light penetration depth than native tissues in the wavelength range 500-900 nm.

Conclusions: Using a PA approach, HIFU-treated tissues interrogated at 720 and 845 nm optical wavelengths can be differentiated from untreated tissues. Based on our spectroscopic investigation, we conclude that the observed PA contrast between HIFU-induced thermal lesions and untreated tissue is due, in part, to the increase in the optical absorption coefficient, the reduced scattering coefficient and, therefore, the deposited laser energy fluence in HIFU-treated tissues.

Key words: high-intensity focused ultrasound (HIFU), thermal lesions, photoacoustic (PA) detection, optical spectroscopy, and optical properties of chicken breast tissue.

I. INTRODUCTION

High-intensity focused ultrasound (HIFU) is a bloodless surgical modality that is capable of inducing thermal and mechanical effects in deep-seated regions of interest (ROI) selectively and non-invasively.[1] Using a high-power focused transducer, HIFU beams can be achieved and focalized within the transducer's focal zone in order to deposit acoustic energy in the ROI with minimal or no harm to intervening tissue layers. Within the ROI, the selectively-deposited acoustic energy is converted into heat, raising the temperature of the targeted tissue volume, while generally keeping the temperature of the surrounding tissue volumes at physiologically safe levels. The increase in the targeted tissue temperature above 56 ^{o}C for at least 1 second can lead to immediate cell death due to protein denaturation in a process known as coagulation necrosis.[2] The spatially-confined, coagulated tissue volumes are termed thermal lesions,[3] since the predominant mechanism of HIFU is thermal, although cavitation and boiling bubbles are also involved in the formation and shaping of the induced thermal lesions,[2] particularly at higher temperatures.

HIFU has been explored for various therapeutic applications including, but not limited to, hemostasis,[4, 5] neurology and pain management,[6] cosmetic surgery,[7] and ophthalmology.[8, 9] Moreover, HIFU therapy demonstrated a great potential for oncological applications including treatments of tumours in the prostate,[10–12] breast fibroadenoma,[13] uterine fibroids,[14, 15] kidney,[12, 16] liver,[12, 17] bladder,[18] bone,[19, 20] and brain.[21, 22] Oncologic and other applications of HIFU are expected to expand with the development of optimized imaging techniques that can provide real-time HIFU treatment monitoring, evaluation, and control.

Currently, most HIFU treatments are monitored and guided with magnetic resonance imaging[11, 13, 14, 17, 19–23] and ultrasound imaging.[24, 25] However, the challenges associated with the

aforementioned imaging modalities, including cost and equipment compatibility with MRI as well as low contrast-resolution between treated and normal tissues with ultrasound imaging, have stimulated the interest of many research groups to investigate alternative HIFU monitoring tools. Among the proposed techniques is photoacoustic (PA) imaging. It is based on the optical absorption of a short, pulsed laser irradiation and the subsequent generation of acoustic waves. These laser-induced acoustic waves, generated as a result of thermo-elastic expansion in the absorbing medium, are detectable by a diagnostic ultrasound transducer.[26] Therefore, PA imaging combines the advantages of both ultrasound and optical imaging modalities, i.e. it provides higher resolution than optical imaging and higher tissue contrast than ultrasound imaging.[26] The higher resolution of PA imaging is due to the weaker ultrasound scattering in tissues than optical scattering.[26] On the other hand, the higher tissue contrast of PA imaging is due to its capability in visualizing the tissue optical absorption properties, providing the advantage of functional imaging of important physiological parameters such as hemoglobin concentration.[26] Moreover, PA imaging is a non-invasive modality that utilizes a non-ionizing electromagnetic radiation.

The possibility of PA detection of HIFU-induced thermal lesions has been demonstrated *in vitro*,[27, 28] *ex vivo*,[29] and *in vivo*.[30] Moreover, previous studies have also been successful in detecting laser-induced thermal lesions photoacoustically.[31, 32] Because the generated PA pressure depends on the absorbed optical energy (i.e. the product of laser energy fluence and optical absorption coefficient) and the thermo-acoustic efficiency of the absorbing structure, a change in at least one of these factors can result in a change in the detected PA signal. Therefore, thermally-induced changes in the optical[33–36] and thermo-mechanical[37, 38] properties of tissues have been investigated following laser-induced thermotherapy or water/saline-bath

heating. However, to our knowledge, the optical and thermo-mechanical properties of HIFU-treated tissues have not yet been examined in conjunction with PA detection of HIFU treatments. In this work, we demonstrate the possibility of PA detection of HIFU-induced thermal lesions in chicken breast tissues *in vitro* at 720 nm and 845 nm laser illuminations. Moreover, for the first time, we measure the optical properties (total transmittance, diffuse reflectance, absorption coefficient, reduced scattering coefficient, effective attenuation coefficient, and light penetration depth) of HIFU-induced thermal lesions and compare them with native (untreated) tissues in the wavelength range of 500-900 nm. The aforementioned objectives are intended to test our hypothesis that PA detection of HIFU-induced thermal lesions is feasible due, in part, to changes in the optical properties of HIFU-treated tissues.

II. MATERIALS AND METHODS

II. A. The HIFU transducer and its driving electronics

A single-element, spherically-concaved HIFU transducer (6699A101, Imasonic S. A.,Voray-sur-l'Ognon, France) made of a high-power piezo-composite material was used in this study. The transducer had a resonance frequency of 1 MHz, aperture diameter of 125 mm, and radius of curvature of 100 mm. It was calibrated using a needle hydrophone (HNA-0400, ONDA Corporation, Sunnyvale, CA) as well as a radiation force balance unit (RFB-2000, ONDA Corporation, Sunnyvale, CA).[39] The transducer's efficiency (ratio of measured output acoustic power to the net input electric power) was determined to be approximately 0.64 (Ref. [39]) for the net input electric power used in this study, which was approximately 110 W.

The HIFU transducer was driven by an arbitrary function generator (AFG3022B, Tektronix, Beaverton, OR), which generated electrical radio-frequency (RF) signals. An RF

power amplifier (A150, Electronics & Innovation, Rochester, NY) was utilized to amplify the generated RF signals. To maximize the transmitted power to the HIFU transducer, a matching network connected the RF power amplifier with the transducer. Moreover, a multi-logger thermometer (HH506RA, OMEGA Engineering Inc., Stamford, CT) was used to monitor the change in the HIFU transducer's surface temperature during treatments, thereby ensuring safe operation of the transducer. A schematic diagram of the experimental setup is shown in Fig. 1.

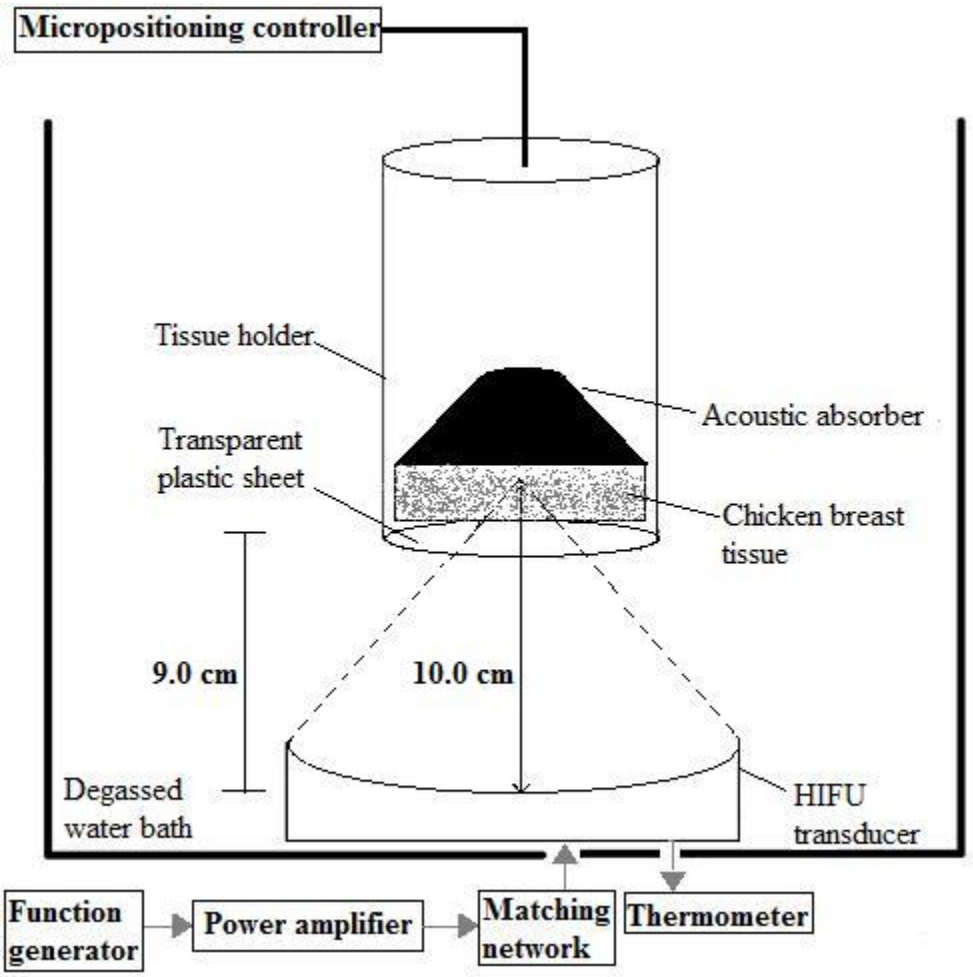

FIG.1. Schematic diagram of the experimental setup of HIFU treatments. The focus of the HIFU transducer was at 10.0 cm. The distance between the centre of the transducer and the transparent plastic sheet covering the opening of the tissue holder was approximately 9.0 cm, resulting in a tissue focal depth of approximately 1.0 cm.

II. B. HIFU treatments

As a biologic tissue model for HIFU treatments, *in vitro* chicken breast tissues, purchased from a local market, were used in this study. After cutting the tissues into approximately 7.5 cm × 6.5 cm × 1.5 cm (length × width × thickness) samples, five HIFU thermal lesions were created in each sample by manually moving the tissue holder using a micropositioning controller (Fig. 1) to five different locations separated by 5 mm. The sequence of generating the five HIFU thermal lesions is illustrated in Fig. 2 (a). The treated region in each sample, which consisted of five HIFU thermal lesions, is shown in Fig. 2 (b).

Operated with 60% duty cycle, the HIFU transducer generated focused waves that propagated through approximately 9.0 cm in degassed water at room temperature (~ 20 ^{o}C) and 1.0 cm in tissue, creating thermal lesions with acoustic intensity, I_{SPTA}, of approximately 1690 W/cm^2 at the transducer's focus inside tissue. The free-field I_{SPTA} was approximately 1910 W/cm^2. The transmitted acoustic power in each HIFU treatment was approximately 42 W, and the total sonication time was 30 seconds.

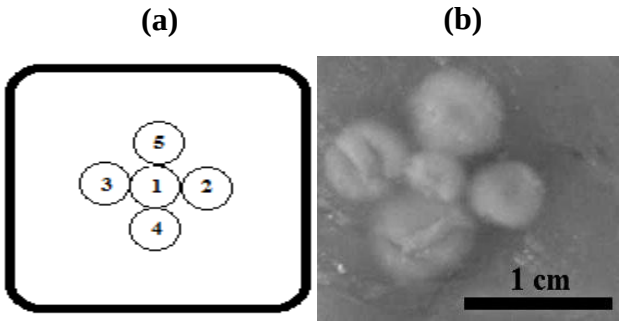

FIG. 2 (a) The sequence followed in creating HIFU thermal lesions. (b) The lateral view of a HIFU-treated chicken breast tissue, cut at the focal plane, showing the induced HIFU lesions. Skin and intervening tissue layers were removed.

II.C. Photoacoustic detection

PA detection of HIFU treatments was achieved using the Imagio Small Animal PA imaging system (Seno Medical Instruments Inc., San Antonio, TX). A schematic diagram of the experimental setup is shown in Fig. 3.

The utilized PA imaging system consisted of a pulsed titanium:sapphire ($Ti:Al_2O_3$) laser with wavelengths tunable in a range between 720 nm and 850 nm. Delivered through an articulated arm, the pulsed laser had a 9-mm beam diameter, 6-ns pulse width, and 10-Hz pulse repetition rate.

The photoacoustic receiver of the PA imaging system was a 4-element annular array ultrasound transducer with a centre frequency of 5 MHz. The -6 dB bandwidth of the transducer was 60% and its focal length was 29.5 mm, as determined previously.[40] The transducer, which had a depth of field of approximately 10 mm, was coaxially mounted at a distance of 105 mm from the laser source in order to allow raster scanning of the chicken breast sample under investigation, which was placed within the transducer's depth of field (Fig. 3). A 52-micron-thick, PVDF-based gold foil (210037022, Measurement Specialities Inc., Hampton, VA) was used to protect the ultrasound transducer from direct laser exposure. Moreover, a CCD camera, placed underneath the ultrasound transducer, was utilized to facilitate targeting of the ROI by the laser beam.

Prior to performing the PA detection experiments, the HIFU-treated chicken breast samples were cut into approximately 4.0 cm × 3.0 cm (width × length) and were sliced to approximately 0.5 cm thickness using a professional food slicer (1060-C, The Rival Company, El Paso, TX). Slicing the chicken breast samples eliminated the undesired skin part of the tissue.

Moreover, in order to prevent contamination of the water tank, the samples were plastic wrapped and vacuum sealed with a vacuum sealer (V2060 FoodSaver, Jarden Corp., Rye, NY). The plastic-wrapped, vacuum-sealed samples were then attached to a tissue holder and placed within the focal zone of the ultrasound transducer inside the PA imaging system's water reservoir (Fig. 3). To compare the PA response of HIFU-treated and native tissues, two ROIs were identified in each one of the 7 samples examined in this study. One of the ROIs was within a HIFU-treated tissue volume while the other ROI was within a native tissue volume in the sample under investigation. Horizontal raster scanning was performed with 0.1 mm scan resolution covering 11 locations within each ROI. The laser fired 4 pulses at each location in the ROI and the detected PA RF signals, which were collected within 0.4 sec, were averaged to generate a single PA RF line. Therefore, a total of 11 PA RF lines, obtained from 11 locations, were recorded for each ROI within each sample. The acquired PA data were imported to MATLAB (R2012b, The MathWork Inc., Natick, MA) for processing. For each one of the 7 samples, the 11 PA RF lines were averaged, producing a single PA RF line that corresponds to a particular ROI (treated or native) within that sample. This averaging method was performed since the samples were well-controlled/stable and uniform, i.e. they did not produce notable variations in space or time within the examined regions. The PA detection experiments were performed with two laser wavelengths: 720 nm and 845 nm, thereby covering the maximum range of wavelengths generated by our PA imaging system.

It is noteworthy to mention that the PA detection experiments were conducted after assessing the accuracy of the charge-coupled device (CCD) camera in targeting the position of a ROI (Fig. 3) using carbon rods, which are known to produce very strong PA signals. Based on the strength of the acquired PA signals, this testing allowed us to make subtle adjustments in the

position of the CCD camera so that the ROI, shown in the real-time CCD camera's image, was coincident with the area that was irradiated by the laser beam.

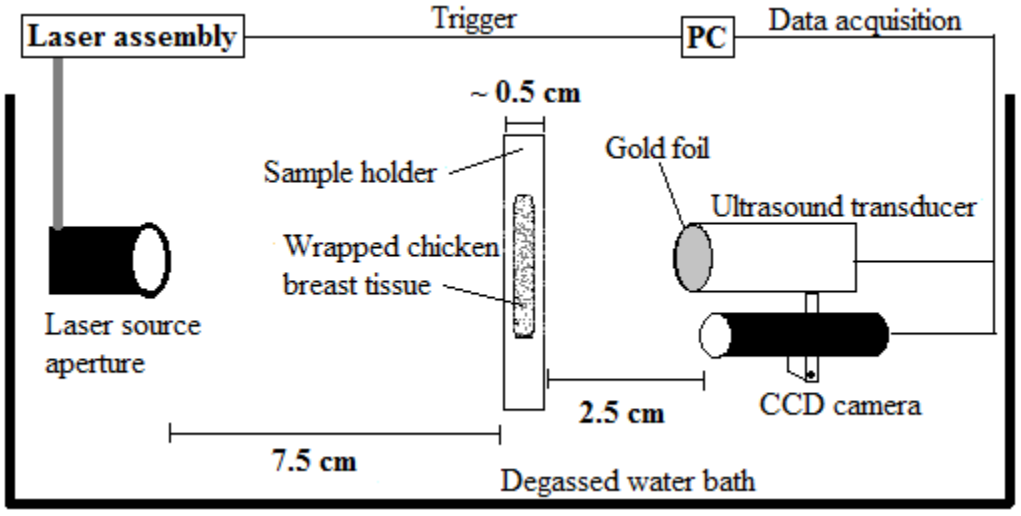

FIG.3. Schematic diagram of the experimental setup of PA detection. In this diagram, the connection between the laser source aperture and the laser assembly does not depict the actual articulated arm for laser beam delivery.

II.D. Optical spectroscopy

Optical spectroscopy experiments were conducted in this study in order to understand the influence of HIFU-induced changes in the optical properties on the detected PA pressure rise, $\Delta P(z)$. The PA pressure rise is directly proportional to the absorbed optical energy and the thermo-acoustic efficiency, and is given in the equation below[41, 42]:

$$\Delta P(z) = \Gamma\, E_{abs}(z) \;=\; \Gamma\, \mu_a \Psi(z) \qquad (1)$$

where Γ is the dimensionless Grüneisen parameter, which represents the fraction of thermal energy that is converted into acoustic waves (also known as thermo-acoustic efficiency). In Eq. (1), the absorbed optical energy from a laser source, $E_{abs}(z)$ [J/m^3], is the product of the optical absorption coefficient, μ_a [m^{-1}], and the laser energy fluence, $\Psi(z)$ [J/m^2].

Our spectroscopic investigation included measurements of diffuse reflectance (DR) and total transmittance (TT) of chicken breast tissue slices, prepared as described in section II.D.1, using a commercially-available spectrophotometer with an integrating sphere attachment (section II.D.2). The inverse adding-doubling method, described in section II.D.3, was utilized to determine the optical absorption coefficient, μ_a, and the reduced scattering coefficient, μ_s', from the experimental data of the DR and TT. The effective attenuation coefficient, μ_{eff}, and the effective light penetration depth, D_{eff}, were calculated in the wavelength range of 500-900 nm using the following equations[41]:

$$\mu_{eff} = \sqrt{3\mu_a(\mu_a + \mu_s')} \tag{2}$$

$$D_{eff} = \frac{1}{\mu_{eff}} \tag{3}$$

II.D.1. Tissue sample preparation

Chicken breast tissues treated with HIFU, as described in II.B, were stored at low temperatures (6-8 ^{o}C) for 12-48 hours prior to conducting optical spectroscopy experiments. Using the food slicer mentioned in section II.C, the tissues were sliced to thin slices; each containing HIFU-treated and native tissue regions. The sliced tissue specimens were further trimmed with a knife to fit within a 1-mm spacing between two 1-mm-thick optical glass slides (BK7, Esco Optics Inc., Oak Ridge, NJ), which were spaced apart using stainless steel shims. Sandwiching sliced tissue specimens within the two optical glass slides reduced the tissue surface irregularities. The tissue specimen and the two optical glass slides covering it had a combined thickness of approximately 3 mm, as measured using a micrometer. Figure 4 is a photograph of one of the 10 sliced tissue specimens that were prepared during our optical spectroscopy experiments.

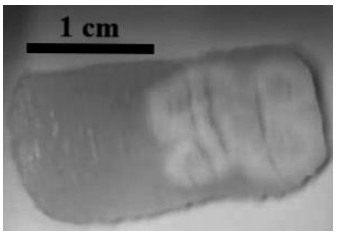

FIG.4. An approximately 1-mm-thick slice of a chicken breast tissue, containing HIFU-treated and native ROIs, used in the optical spectroscopy experiments.

II.D.2. Integrating-sphere measurements

To compare the optical properties of HIFU-treated and native tissues, the sliced tissue specimens, which were positioned between two optical glass slides, were used in optical spectroscopy experiments using the Shimadzu spectrophotometer (UV 3600 UV-VIS-NIR, Shimadzu Scientific Instruments, Columbia, MD) with the ISR-3100 integrating sphere attachment. The system's sphere diameter was 60.0 mm, entrance port diameter was 16.7 mm, and the exit port diameter was 18.8 mm. The integrating-sphere method allowed us carry out the DR and TT measurements in a dual-beam mode, with a single-integrating-sphere configuration. The utilized slit width, which was fixed during the experiments, was 8 nm, yielding a measured illumination beam of approximately 7.1 mm at the sample surface. The wavelength of grating and detector changes was set at 910 nm. The experimental setup of the DR and TT measurements is depicted in Figs. 5 and 6, which were reproduced, with permission, from Shimadzu Corporation.[43, 44]

A total of 10 sliced tissue specimens were prepared as described in section II.D1. For each one of the 10 sliced tissue specimens, the DR and TT of native and HIFU-treated portions of the tissue were measured three times between 500 nm and 900 nm in 1-nm increments. Therefore, for a given sliced tissue specimen, four spectra were generated, each of which was an average of three trials. These spectra were: (a) TT and DR for the native portion of a specimen

(two spectra), and (b) TT and DR for the HIFU-treated portion of a specimen (two spectra).

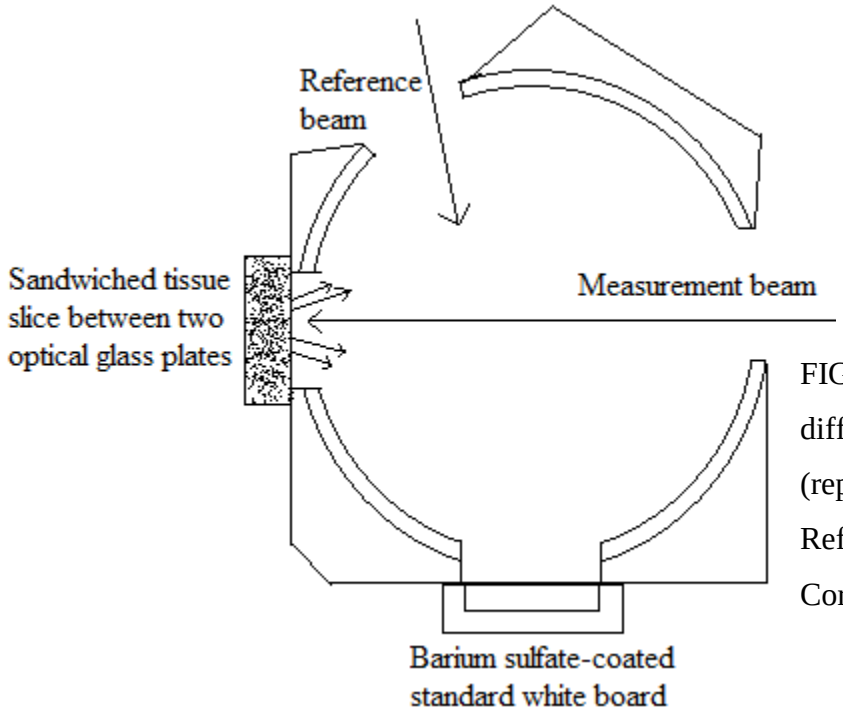

FIG.5. Diagram of a dual-beam diffuse reflectance measurement (reproduced, with permission, from Ref [43]; courtesy of Shimadzu Corporation).

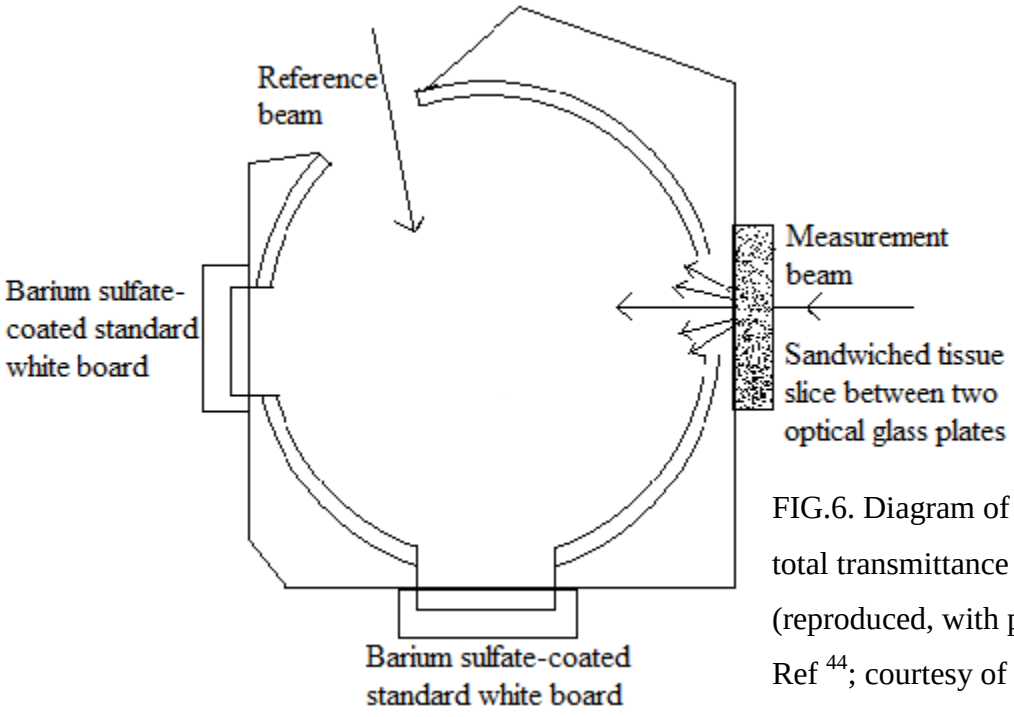

FIG.6. Diagram of a dual-beam total transmittance measurement (reproduced, with permission, from Ref [44]; courtesy of Shimadzu Corporation).

II.D.3. Inverse adding-doubling method

The inverse adding-doubling (IAD) program[45, 46] was employed in this study to determine the optical absorption and the reduced scattering coefficients of HIFU-treated and native chicken breast tissues using the DR and TT data, collected as described in section II.D.2. In the IAD program, optical parameters such as scattering, absorption, and scattering anisotropy can be determined by repeatedly solving the radiative transport equation (RTE) until a match with the measured reflection and transmission values is made.[45] The "inverse" implies a reversal to the regular extraction of transmission and reflection values from the optical properties, whereas "adding-doubling" refers to the utilized methodology in solving the RTE.[45] The IAD is a versatile method, and is well-suited for measurements employing biologic tissue specimens positioned between optical glass slides.[45]

III. RESULTS AND DISCUSSION

III.A. PA detection of HIFU-induced thermal lesions

Figures 7 and 8 show the PA RF signals of 7 samples at 720 and 845 nm laser illumination, respectively, averaged from 11 locations within each ROI in the HIFU-treated and native tissue volumes of each sample. The numerical values that appear inside the rectangular boxes placed within each one of the 14 PA RF lines of Figs. 7 and 8 represent the ratio of the peak-to-peak PA signal amplitudes of HIFU-treated and native ROIs of their respective sample-wavelength combination. Combining the ratios of the 7 samples investigated at 720 nm, the averaged ratio of the peak-to-peak PA signal amplitude of HIFU-treated tissue to that of native tissue is 3.68 ± 0.25 (mean ± SEM). At 845 nm, the averaged ratio of the peak-to-peak PA signal amplitude of HIFU-treated tissue to that of native tissue is 3.75 ± 0.26 (mean ± SEM).

Figure 9 provides a comparison of the averaged ratios of the HIFU-treated and native tissue peak-to-peak PA signal amplitudes from the 7 samples at 720 and 845 nm laser illumination. The increase in the PA signal amplitude by more than 3 times as a result of HIFU-induced coagulation has also been reported in a previous study.[28] It is important to note that HIFU-induced thermal lesions have a higher acoustic attenuation coefficient than native tissues.[47, 48] Therefore, laser-generated PA pressure waves should undergo a greater acoustic attenuation as they propagate through a thermal lesion compared to native tissue. The effect of the increased ultrasound attenuation is expected to be more pronounced in the PA detection geometry of Fig. 3, for which the laser source aperture and the ultrasound transducer are on opposite ends of the sample. Nevertheless, the detected PA signals from HIFU-induced thermal lesions had greater peak-to-peak amplitudes than native tissues. The observed PA contrast between HIFU-treated and native tissues implies that the PA method can indeed detect HIFU-induced thermal lesions at 720 and 845 nm laser illuminations. An understanding of how the detected PA pressure (Eq. 1) is influenced by HIFU-induced changes in the optical properties is necessary in order to explain the observed PA contrast in Figs. 7 and 8.

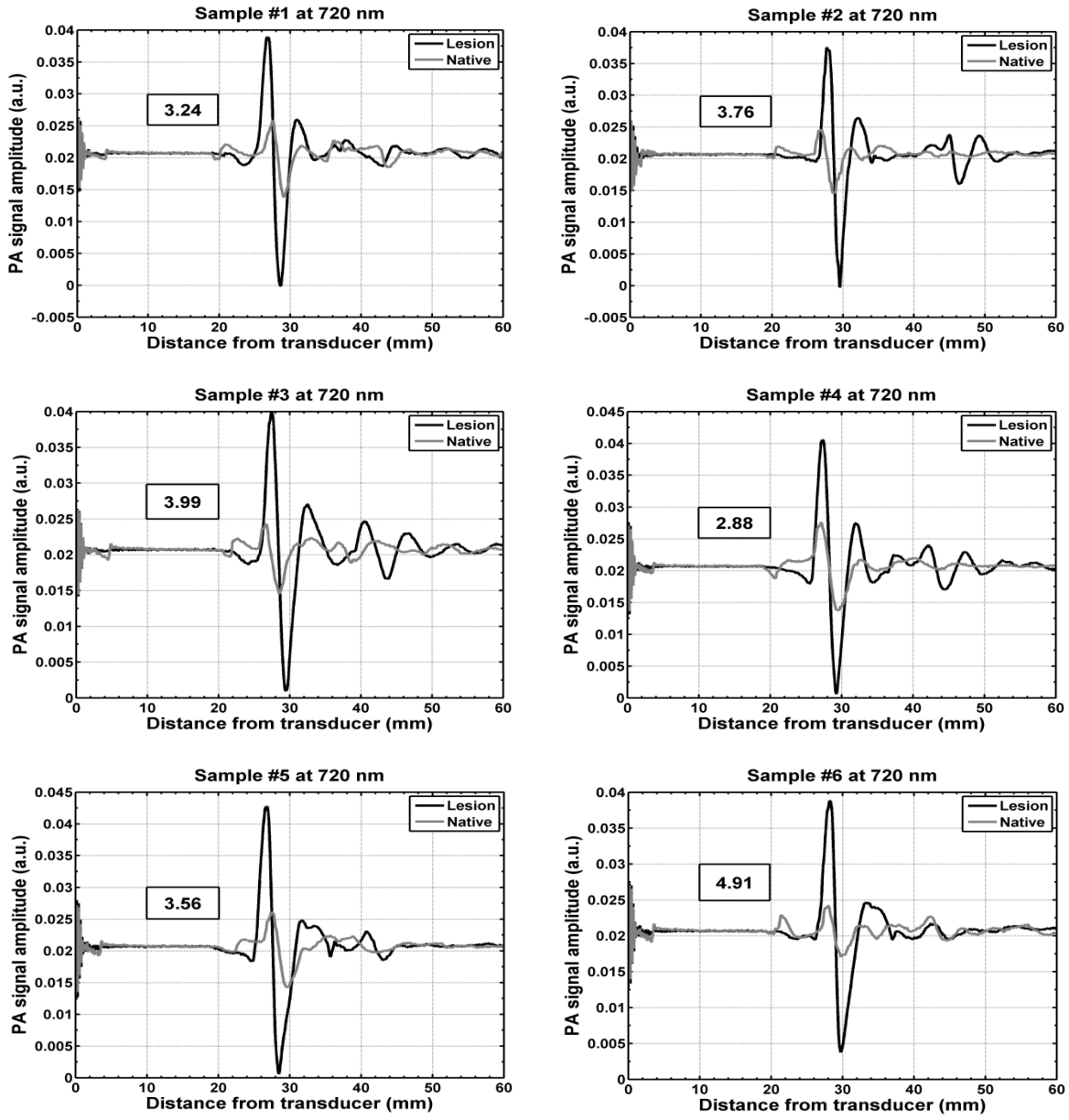

FIG.7. Photoacoustic RF lines obtained from 7 chicken breast samples irradiated at 720 nm. Within a given sample, the lesion and native RF lines represent the average of the RF lines collected at 11 locations within a HIFU-treated and native ROIs, respectively. The numerical values inside the boxes represent the ratio of the averaged peak-to-peak signal amplitudes of HIFU-treated and native ROIs of their respective samples.

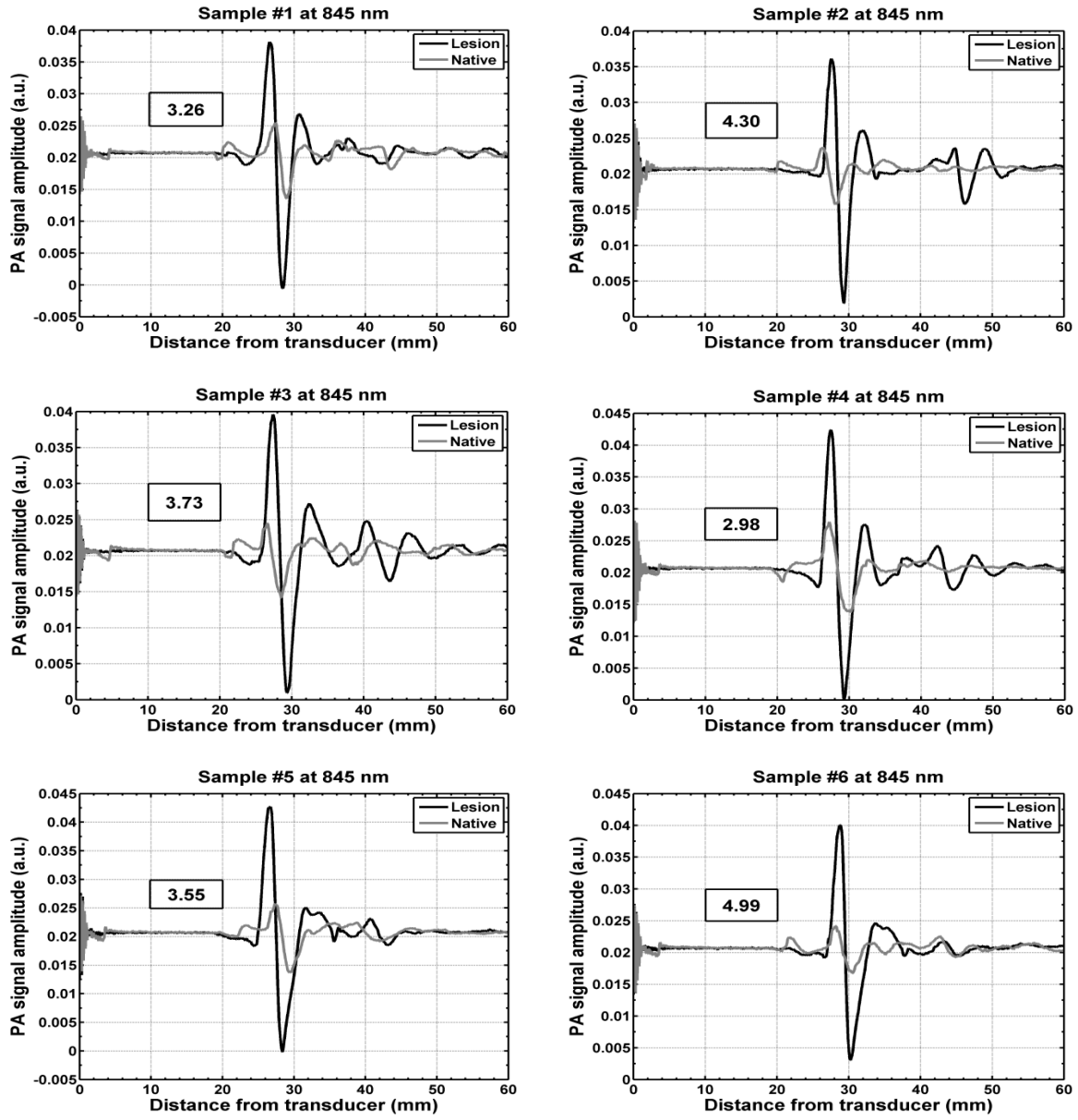

FIG.8. Photoacoustic RF lines obtained from 7 chicken breast samples irradiated at 845 nm. Within a given sample, the lesion and native RF lines represent the average of the RF lines collected at 11 locations within a HIFU-treated and native ROIs, respectively. The numerical values inside the boxes represent the ratio of the averaged peak-to-peak signal amplitudes of HIFU-treated and native ROIs of their respective samples.

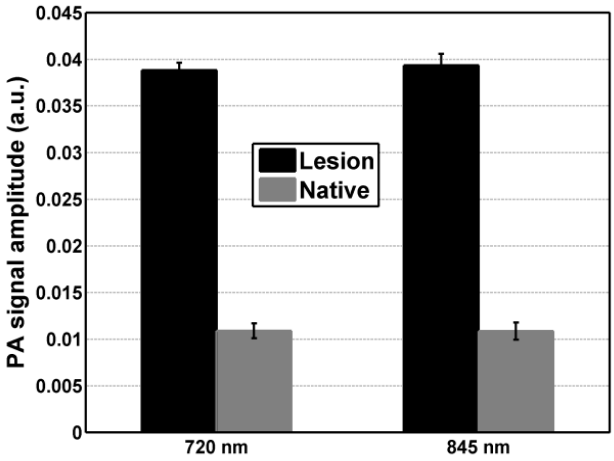

FIG.9. A comparison between averaged ratios of HIFU-treated and native tissue peak-to-peak PA signal amplitudes from the 7 samples obtained at 720 and 845 nm laser illumination. Error bars represent the standard error of the mean (SEM).

III.B. Optical spectroscopy of HIFU-treated and native tissues

III.B.1. Diffuse reflectance and total transmittance

Figure 10 shows the averaged results of the integrating-sphere measurements on 10 chicken breast tissue slices. In Fig. 10 (a) and (b), the TT and DR spectra are presented, respectively, with the SEM for both HIFU-treated and native tissues in the wavelength range of 500-900 nm. The TT and DR results provide a quantitative comparison between HIFU-treated and native tissues in terms of their wavelength-dependent ability to reflect and transmit light between 500 to 900 nm. Figure 10 (a) shows that the ratio of TT of native tissue to that of HIFU-treated tissue ranges from 5.54 to 6.66 in the wavelength range of 500-550 nm. However, this ratio tends to gradually decrease as the wavelength increases, reaching a value of 2.74 at 900 nm. Figure 10 (b) shows that the ratio of DR of HIFU-treated tissue to that of native tissue increases from about 3.09 at 500 nm to about 3.97 at 900 nm. Figures 10 (a) and (b) show that the wavelength range of 630-900 nm is appropriate for optical diagnostics of HIFU-treated and native chicken breast tissues *in vitro* because light has a relatively high transmittance and low

reflectance in this range. This observation will be confirmed later with the effective light penetration depth graph.

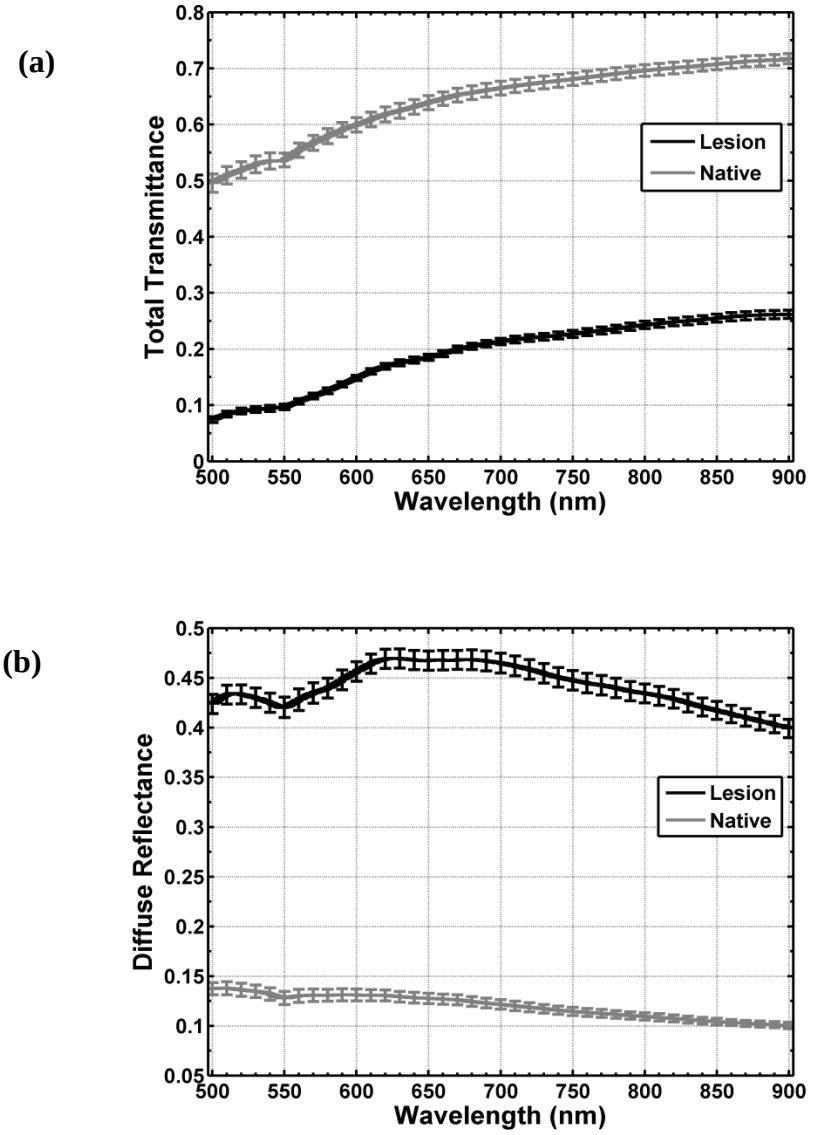

FIG.10. Results of the integrating-sphere measurements. (a) and (b) the averaged total transmittance and diffuse reflectance with the SEM, respectively, of HIFU-treated and native tissues in the wavelength range of 500-900 nm.

III.B.2. Optical absorption and reduced scattering coefficients

Using the IAD program,[46] the optical absorption coefficient and the reduced scattering coefficient spectra were determined for each one of the 10 tissue slices. Figures 11 (a) and (b) show the averaged optical absorption coefficient and the reduced scattering coefficient spectra, respectively, with the SEM for both HIFU-treated and native tissues in the wavelength range of 500-900 nm. Figure 11 (a) shows that the optical wavelength range of approximately 670-900 nm has the lowest absorption coefficient for HIFU-treated and native chicken breast tissue, making it an appropriate range for optical diagnostics of relatively deep-seated ROIs. As per Eq. 1, the difference in the optical absorption coefficients of HIFU-treated and native tissues in the aforementioned optical wavelength range is a contributor to the difference in the PA response detected from HIFU-treated and native tissues at 720 nm and 845 nm. In other words, the HIFU-induced increase in the PA signal amplitudes (Figs. 7 and 8) can be attributed, in part, to the increased optical absorption coefficients of HIFU-treated tissues as compared to native tissues. Figure 11 (b) shows the large difference between the reduced scattering coefficients of HIFU-treated and native tissues. In fact, at 500 nm, the ratio of the reduced scattering coefficients of HIFU-treated tissue to that of native tissue is approximately 11.19, while at 900 nm the ratio increases to about 15.42. The general decrease in the reduced scattering coefficient spectra of both HIFU-treated and native tissues with wavelength, as depicted in Fig. 11 (b), is consistent with a previous work that utilized saline-bath heating of tissues.[36] Although they did not use HIFU treatments in their investigation, Yaroslavsky et al.[36] obtained results that are consistent with ours as they have also reported a thermally-induced increase in μ_a and μ_s' of saline-bath-treated brain tissues, compared with native brain tissues.[36]

The observed increase in μ_a of HIFU-treated tissues (Fig. 11 (a)) may be attributable, in part, to the thermally-induced formation of methemoglobin, a form of hemoglobin with its iron being in the ferric oxidation state, in the blood.[49] The formation of methemoglobin results in an enhanced optical absorption coefficient of the thermally-coagulated blood,[49] as compared to native blood, within the wavelength range investigated in our study. Similarly, the increase in μ_s' of HIFU-treated tissue may be explained by the increase in μ_s' of thermally-coagulated blood compared to native blood.[49] It is noteworthy to mention that the visual appearance of the chicken breast tissues (i.e. their pink color) as well as their optical absorption spectrum, which resembles that of blood,[50] attest the presence of hemoglobin in our samples. A similar argument about the presence of blood residuals in excised tissue samples was made in previous studies that utilized liver[27] and brain[36] tissues. However, due to the low blood content in our tissue samples, the thermally-induced formation of methemoglobin might not have had a major contribution to the HIFU-induced changes in the optical properties of the tissue samples. Other factors, discussed in the next paragraph, might have resulted in greater changes in the optical properties. These factors include protein coagulation and dehydration (i.e. water loss).

Protein coagulation and dehydration might have been major reasons behind the changes in the optical properties of HIFU-treated tissues. Firstly, thermal denaturation, which causes functional and structural alterations in the heated proteins, results in the production of highly-scattering, amorphous granules to replace well-structured, highly-organized molecules, present prior to heating.[51] The appearance of the small, thermally-denatured granular proteins may be a key factor in the increase in the reduced scattering coefficient of thermally-coagulated tissues, based on analyses relying on Mie theory.[52] Secondly, dehydration and tissue shrinkage have been shown to increase the optical absorption coefficient of biologic tissues.[53] Moreover, by the virtue

of decreasing the overall coagulated tissue volume, dehydration and tissue shrinkage may also result in an increase in the concentration of optical attenuators (scattering and absorbing centres).[36] Therefore, HIFU-induced dehydration of the treated tissue volume can be an important contributor to the increased optical scattering and absorption of the HIFU-induced thermal lesions in the wavelength range investigated in our experiments.

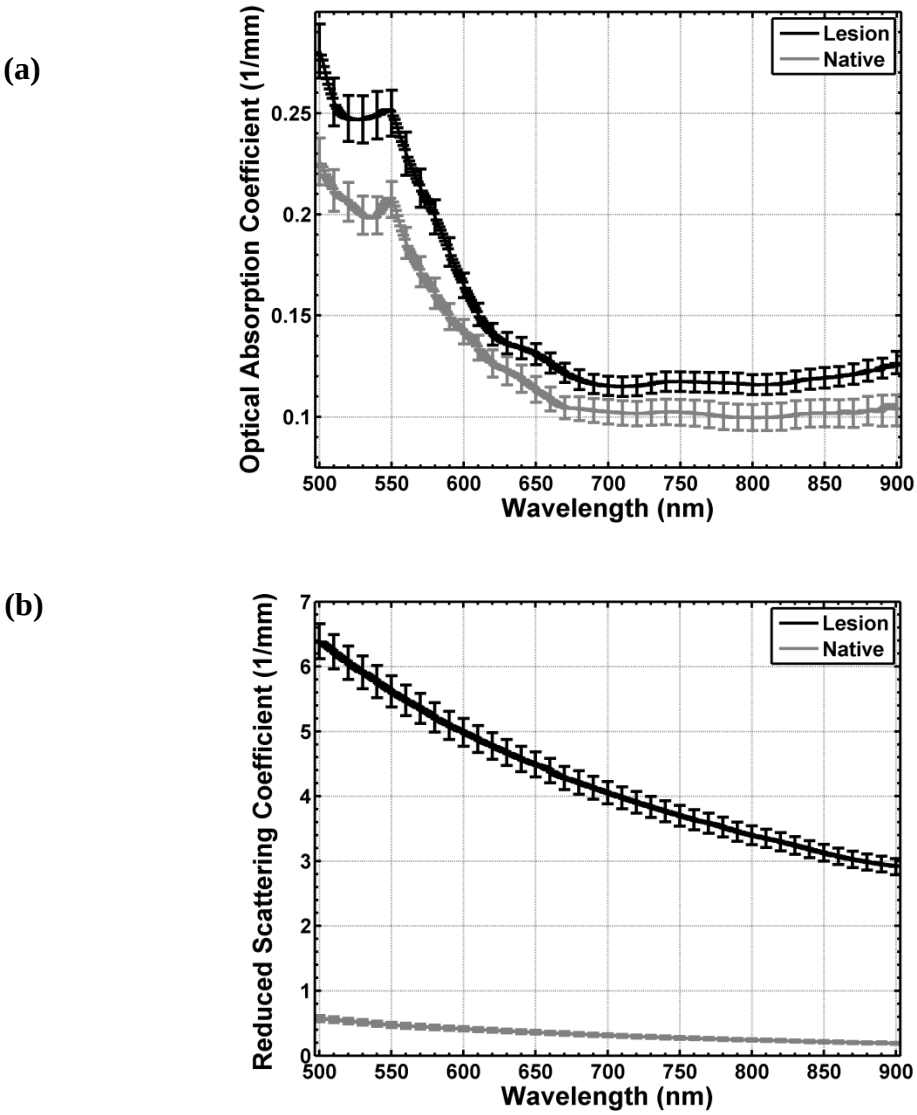

FIG. 11. Results of the IAD computations. (a) and (b) the averaged optical absorption coefficients and reduced scattering coefficients with the SEM, respectively, of HIFU-treated and native chicken breast tissues in the wavelength range of 500-900 nm.

III.B.3. Effective attenuation coefficient and light penetration depth

Using Eqs. 2 and 3, the wavelength-dependent effective attenuation coefficients and light penetration depths were determined, respectively, for each one of the 10 chicken breast tissue slices. Figures 12 (a) and (b) show the averaged effective attenuation coefficient and the averaged light penetration depth graphs, respectively, with the SEM for both native and HIFU-treated tissues in the wavelength range of 500 – 900 nm. The gradual decrease in the effective attenuation coefficient and the increase in the effective light penetration depth between 630- 900 nm in Figs. 12 (a) and (b), respectively, attest to our previous statement about this range being well-suited for *in vitro* optical diagnostics of HIFU-treated and native chicken breast tissues.

Comparing the effective attenuation coefficient and the light penetration depth of HIFU-treated and native tissues can provide an explanation as to why the averaged PA signal amplitudes detected from HIFU-treated tissues were greater than those of native tissues. A superficial HIFU-induced thermal lesion with a lower light penetration depth (i.e. higher effective attenuation coefficient) attenuates greater amount of the incident laser energy than a superficial native tissue of the same volume. In other words, within a HIFU-treated tissue volume, there is a greater probability of photon interactions than a native tissue of the same volume, reducing the light penetration depth and increasing its propagation duration inside the coagulated tissue. Consequently, the amount of the laser energy that is deposited within a HIFU-treated tissue is greater than that within a native tissue, producing a stronger PA pressure rise due to an increase in the laser energy fluence (Eq. 1).

In summary, within the volume of a HIFU-induced thermal lesion, there are greater light-tissue interactions (scattering and absorption) that decreases the effective light penetration depth

and confines most of its energy (i.e. increases laser fluence) within the lesion's volume, thereby producing greater PA signal amplitudes than native tissues.

(a)

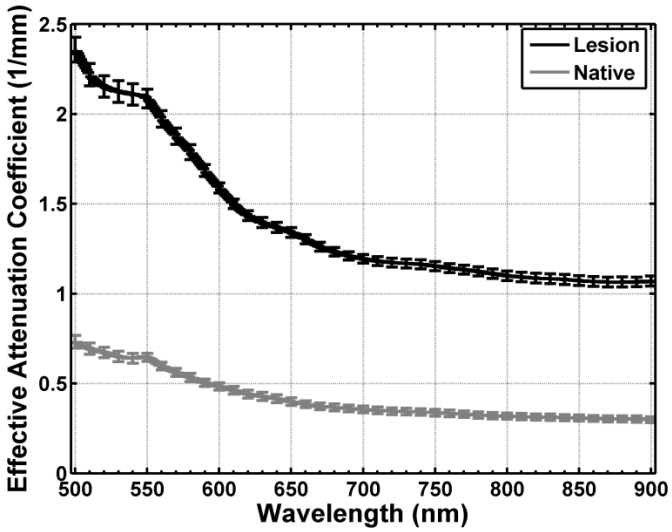

(b)

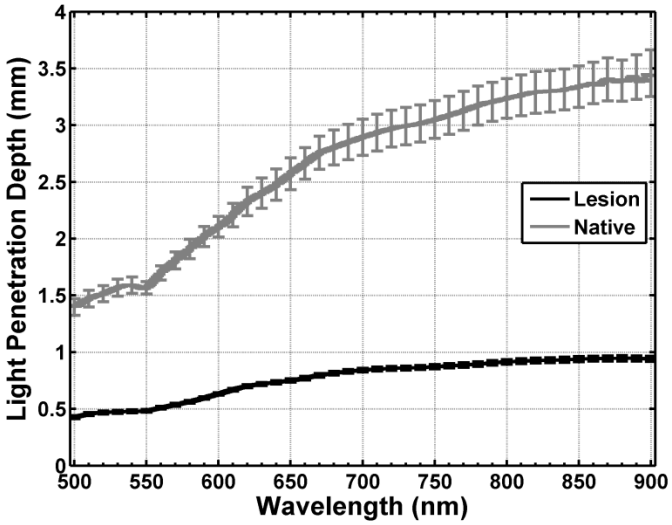

FIG. 12. Results of applying equations 2 and 3. (a) and (b) the averaged effective attenuation coefficient and effective light penetration depth graphs with the SEM, respectively, of HIFU-treated and native chicken breast tissues in the wavelength range of 500-900 nm.

IV. CONCLUSION

In this study, we have successfully demonstrated the feasibility of PA detection of HIFU-induced thermal lesions in chicken breast tissues *in vitro* at 720 and 845 nm laser illuminations. A more than three-fold increase was observed in the PA signal amplitudes of HIFU-treated tissues compared to native (i.e. untreated) tissues at 720 and 845 nm optical wavelengths, indicating that PA method is indeed capable of detecting HIFU-induced tissue coagulation necrosis and its associated alterations in the molecular and structural compositions of tissues. In order to assist in the interpretation of the aforementioned PA contrast between HIFU-treated and native tissues, we have determined, for the first time, the optical properties of HIFU-induced thermal lesions and compared them with native tissues by performing optical spectroscopy in the wavelength range of 500-900 nm. Based on Eq. (1), our spectroscopic investigation has shown that there are direct and indirect optical factors that together contributed to the observed enhancement in the PA pressure as a result of HIFU-induced thermal lesions. The direct optical factor is the increase in the optical absorption coefficient of the HIFU-treated tissue. The indirect optical factor is the large increase in the reduced scattering coefficient, which contributed to an increase in the effective optical attenuation coefficient and a decrease in the light penetration depth. Hence, the increase in the reduced scattering coefficient has indirectly enhanced the PA pressure rise by increasing the absorbed optical energy (Eq. 1). For a complete analysis of the effects of the parameters in Eq. (1) on the detected PA pressure, assessment of the contribution of thermo-acoustic efficiency (Grüneisen parameter) of HIFU-induced thermal lesions on the detected pressure rise should be studied in biologic tissues. It is also suggested to extend this work to a more-clinically relevant scenario by using an *in vivo* animal model. The blood content in *in vivo* animal models will have an important role on the generated PA signals from HIFU-

treated and native tissues. If methemoglobin is formed in the blood,[30] it is anticipated that the generated PA signals could have greater amplitudes for HIFU-treated tissues compared to native tissues because of the reasons discussed in section III.B.2. On the other hand, if methemoglobin is not formed in the blood, it is expected, as shown in a previous work[30], that HIFU-induced thermal coagulation could potentially result, depending on the optical illumination wavelength, in a reduction in the PA signal amplitude in regions where there is a large amount of blood, particularly due to reduction of blood plasma and the coagulation of red blood cells in the HIFU-treated region.

Acknowledgment

The authors would like to thank Dr. Alexandre Douplik for fruitful discussions during this project. Arthur Worthington, Martin Hohmann, and Eno Hysi are gratefully acknowledged for assistance and technical support. This work was partially supported by the Ontario Research Fund- Research Excellence (ORF-RE) grant and the Natural Science and Engineering Research Council of Canada (NSERC Discovery grant) that were awarded to Drs. J. Tavakkoli and M. C. Kolios. A Natural Science and Engineering Research Council of Canada Research Tools and Instrumentation (RTI) grant awarded to Dr. M. C. Kolios supported the purchase of the Shimadzu spectrophotometer used in this study.

Bibliography

[1] S. Vaezy, M. Andrew, P. Kaczkowski, and L. Crum, "Image-guided acoustic therapy," Annual Review of Biomedical Engineering **3**, 375–390 (2001).

[2] C.R. Hill and G.R. ter Haar, "High intensity focused ultrasound -- potential for cancer treatment," British Journal of Radiology **68**, 1296–1303 (1995).

[3] G. ter Haar and C. Coussios, "High intensity focused ultrasound: physical principles and devices," International Journal of Hyperthermia **23**, 89–104 (2007).

[4] S. Vaezy, R. Martin, P. Kaczkowski, G. Keilman, B. Goldman, H. Yaziji, S. Carter, M. Caps, and L. Crum, "Use of high-intensity focused ultrasound to control bleeding," Journal of Vascular Surgery **29**, 533–542 (1999).

[5] S. Vaezy *et al.*, "Liver hemostasis using high-intensity focused ultrasound," Ultrasound in Medicine & Biology **23**, 1413–1420 (1997).

[6] J.L. Foley, S. Vaezy, and L.A. Crum, "Applications of high-intensity focused ultrasound in medicine : Spotlight on neurological applications," Applied Acoustics **68**, 245–259 (2007).

[7] W. White, I. Makin, P. Barthe, M. Slayton, and R. Gliklich, "Selective creation of thermal injury zones in the superficial musculoaponeurotic system using intense ultrasound therapy: A new target for noninvasive facial rejuvenation," Archives of Facial Plastic Surgery **9**, 22–29 (2007).

[8] D. Coleman, F. Lizzi, J. Driller, A. Rosado, S. Chang, T. Iwamoto, and D. Rosenthal, "Therapeutic ultrasound in the treatment of glaucoma. I. Experimental model," Ophthalmology **92**, 339–346 (1985).

[9] D. Coleman, F. Lizzi, J. Driller, A. Rosado, S. Burgess, J. Torpey, M. Smith, R. Silverman, M. Yablonshi, and S. Chang, "Therapeutic ultrasound in the treatment of glaucoma. II. Clinical applications," Ophthalmology **92**, 347–353 (1985).

[10] J. Chapelon, M. Ribault, F. Vernier, R. Souchon, and A. Gelet, "Treatment of localized prostate cancer with transrectal high intensity focused ultrasound," European Journal of Ultrasound **9**, 31–38 (1999).

[11] W.A. N'djin, M. Burtnyk, I. Kobelevskiy, S. Hadjis, M. Bronskill, and R. Chopra, "Coagulation of human prostate volumes with MRI-controlled transurethral ultrasound therapy: results in gel phantoms," Medical Physics **39**, 4524–4536 (2012).

[12] A.G. Visioli, I.H. Rivens, G.R. ter Haar, A. Horwich, R.A. Huddart, E. Moskovic, A. Padhani, and J. Glees, "Preliminary results of a phase I dose escalation clinical trial using

focused ultrasound in the treatment of localised tumours," European Journal of Ultrasound **9**, 11–18 (1999).

[13] K. Hynynen, O. Pomeroy, D.N. Smith, P.E. Huber, N.J. McDannold, J. Kettenbach, J. Baum, S. Singer, and F.A. Jolesz, "MR imaging-guided focused ultrasound surgery of fibroadenomas in the breast: a feasibility study," Radiology **219**, 176–185 (2001).

[14] C.M.C. Tempany, E.A. Stewart, N. McDannold, B.J. Quade, F.A. Jolesz, and K. Hynynen, "MR imaging-guided focused ultrasound surgery of uterine leiomyomas: a feasibility study," Radiology **226**, 897–905 (2003).

[15] E. Stewart *et al.*, "Focused ultrasound treatment of uterine fibroid tumors: Safety and feasibility of a noninvasive thermoablative technique," American Journal of Obstetrics & Gynecology **189**, 48–54 (2003).

[16] R.F. Paterson, E. Barret, T.M. Siqueira, T.A. Gardner, J. Tavakkoli, V. V Rao, N.T. Sanghvi, L. Cheng, and A.L. Shalhav, "Laparoscopic partial kidney ablation with high intensity focused ultrasound," The Journal of Urology **169**, 347–351 (2003).

[17] A. Okada, T. Murakami, K. Mikami, H. Onishi, N. Tanigawa, T. Marukawa, and H. Nakamura, "A case of hepatocellular carcinoma treated by MR-guided focused ultrasound ablation with respiratory gating," Magnetic Resonance in Medical Sciences **5**, 167–171 (2006).

[18] G. Vallancien, M. Harouni, B. Guillonneau, B. Veillon, and J. Bougaran, "Ablation of superficial bladder tumors with focused extracorporeal pyrotherapy," Urology **47**, 204–207 (1996).

[19] D. Gianfelice, C. Gupta, W. Kucharczyk, P. Bret, D. Havill, and M. Clemons, "Palliative treatment of painful bone metastases with MR imaging-guided focused ultrasound," Radiology **249**, 355–363 (2008).

[20] B. Liberman *et al.*, "Pain Palliation in patients with bone metastases using MR-guided focused ultrasound surgery : A multicenter study," Annals of Surgical Oncology **16**, 140–146 (2008).

[21] K. Hynynen, G. Clement, N. McDannold, N. Vykhodtseva, R. King, P. White, S. Vitek, and F. Jolesz, "500-element ultrasound phased array system for noninvasive focal surgery of the brain: A preliminary rabbit study with ex vivo human skulls," Magnetic Resonance in Medicine **52**, 100–107 (2004).

[22] K. Hynynen, N. McDannold, G. Clement, F. Jolesz, E. Zadicario, R. Killiany, T. Moore, and D. Rosen, "Pre-clinical testing of a phased array ultrasound system for MRI-guided noninvasive surgery of the brain—A primate study," European Journal of Radiology **59**, 149–156 (2006).

[23] K. Hynynen, "MRI-guided focused ultrasound treatments.," Ultrasonics **50**, 221–229 (2010).

[24] S. Vaezy, X. Shi, R. Martin, E. Chi, P. Nelson, M. Bailey, and L. Crum, "Real-time visualization of high-intensity focused ultrasound treatment using ultrasound imaging," Ultrasound in Medicine & Biology **27**, 33–42 (2001).

[25] J. Tavakkoli and N.T. Sanghvi, "Ultrasound-guided HIFU and thermal ablation," in *Therapeutic Ultrasound: Mechanisms to Applications*, edited by V. Frenkel (Nova Science Publishers, Hauppauge, NY, 2011), pp. 137–161.

[26] M. Xu and L. V Wang, "Photoacoustic imaging in biomedicine," Review of Scientific Instruments **77**, 041101 (2006).

[27] T. Khokhlova, I.M. Pelivanov, O.A. Sapozhnikov, V.S. Solomatin, and A.A. Karabutov, "Opto-acoustic diagnostics of the thermal action of high-intensity focused ultrasound on biological tissues: the possibility of its applications and model experiments," Quantum Electronics **36**, 1097–1102 (2006).

[28] H. Cui and X. Yang, "Real-time monitoring of high-intensity focused ultrasound ablations with photoacoustic technique: an in vitro study," Medical Physics **38**, 5345–5350 (2011).

[29] Y. Sun and B.O. Neill, "Imaging high-intensity focused ultrasound-induced tissue denaturation by multispectral photoacoustic method: an ex vivo study," Applied Optics **52**, 1764–1770 (2013).

[30] P. Chitnis, H. Brecht, R. Su, and A. Oraevsky, "Feasibility of optoacoustic visualization of high-intensity focused ultrasound-induced thermal lesions in live tissue," Journal of Biomedical Optics **15**, 021313 (2010).

[31] K. Larin, I. Larina, and R. Esenaliev, "Monitoring of tissue coagulation during thermotherapy using optoacoustic technique," Journal of Physics D: Applied Physics **38**, 2645–2653 (2005).

[32] M. Arsenault, M. Kolios, and W. Whelan, "Optoacoustic detection of thermal lesions," Proc. SPIE **7177**, 71771V (2009).

[33] J. Ritz, A. Roggan, C. Isbert, G. Muller, H. Buhr, and C. Germer, "Optical properties of native and coagulated porcine liver tissue between 400 and 2400 nm," Lasers in Surgery and Medicine **29**, 205–212 (2001).

[34] A.M.K. Nilsson, C. Sturesson, D.L. Liu, and S. Andersson-Engels, "Changes in spectral shape of tissue optical properties in conjunction with laser-induced thermotherapy," Applied Optics **37**, 1256–1267 (1998).

[35] K. Ishii, A. Kimura, and K. Awazu, "Optical properties of tissues after laser treatments in the wavelength range of 350 - 1000 nm," Proc. SPIE **6991**, 69912F (2008).

[36] A. Yaroslavsky, P. Schulze, I. Yaroslavsky, R. Schober, F. Ulrich, and H.-J. Schwarzmaier, "Optical properties of selected native and coagulated human brain tissues in vitro in the visible and near infrared spectral range," Physics in Medicine & Biology **47**, 2059–2073 (2002).

[37] B. Soroushian, W.M. Whelan, and M.C. Kolios, "Study of laser-induced thermoelastic deformation of native and coagulated ex-vivo bovine liver tissues for estimating their optical and thermomechanical properties," Journal of Biomedical Optics **15**, 065002 (2010).

[38] B. Soroushian, W.M. Whelan, and M.C. Kolios, "Dynamics of laser induced thermoelastic expansion of native and coagulated ex-vivo soft tissue samples and their optical and thermo- mechanical properties," Proc. SPIE **7899**, 78990Z (2011).

[39] S. Rahimian, An Acoustic Backscatter-Based Method for Estimating Attenuation Towards Monitoring Lesion Formation in High Intensity Focused Ultrasound (Ryerson University, 2012).

[40] E. Hysi, R.K. Saha, and M.C. Kolios, "Photoacoustic ultrasound spectroscopy for assessing red blood cell aggregation and oxygenation," Journal of Biomedical Optics **17**(12), 125006 (2012).

[41] A.A. Oraevsky, S.L. Jacques, and F.K. Tittel, "Determination of tissue optical properties by piezoelectric detection of laser-induced stress waves," in *Laser-Tissue Interaction IV*, edited by S.L. Jacques and A. Katzir (Proc. SPIE 1882, 86-101, 1993).

[42] V.E. Gusev and A.A. Karabutov, *Laser Optoacoustics* (American Institute of Physics, New York, 1992).

[43] Shimadzu Corporation, *Diffuse reflectance measurement*, (2013).

[44] Shimadzu Corporation, *Transmittance measurement*, (2013).

[45] S.A. Prahl, M.J.C. van Gemert, and A.J. Welch, "Determining the optical properties of turbid media by using the adding-doubling method," Applied Optics **32**, 559–568 (1993).

[46] S.A. Prahl, *Inverse Adding-Doubling program: Version 3-9-6*, (2013). (http://omlc.ogi.edu/software/iad/index.html)

[47] S. Rahimian and J. Tavakkoli, "Estimating dynamic changes of tissue attenuation coefficient during high-intensity focused ultrasound treatment," Journal of Therapeutic Ultrasound **14**, 1–22 (2013).

[48] N. Bush, I. Rivens, G. ter Haar, and J. Bamber, "Acoustic properties of lesions generated with an ultrasound therapy system," Ultrasound in Medicine & Biology **19**, 789–801 (1993).

[49] J. Barton, G. Frangineas, H. Pummer, and J. Black, "Cooperative phenomena in two-pulse, two-color laser photocoagulation of cutaneous blood vessels," Photochemistry & Photobiology **73**, 642–650 (2001).

[50] M. Meinke, G. Müller, J. Helfmann, and M. Friebel, "Optical properties of platelets and blood plasma and their influence on the optical behavior of whole blood in the visible to near infrared wavelength range," Journal of Biomedical Optics **12**, 014024 (2007).

[51] A. Welch and M. van Gemert (eds.), *Optical-thermal response of laser-irradiated tissue*, 2nd ed. (Springer, New York, 2011).

[52] S. Thomsen, S. Jacques, and S. Flock, "Microscopic correlates of macroscopic optical property changes during thermal coagulation of myocardium," Proc. SPIE **1202**, 2–11 (1990).

[53] I.F. Cilesiz and A.J. Welch, "Light dosimetry : Effects of dehydration and thermal damage on the optical properties of the human aorta," Applied Optics **32**, 477–487 (1993).

Chapter 3: Discussions, Conclusions, and Future work

3.1 Discussions

In this work, HIFU treatments were applied to chicken breast tissue *in vitro* using a 1-MHz HIFU transducer. The capability of a PA method to detect HIFU-induced thermal lesions was evaluated by comparing the PA peak-to-peak signal amplitudes of HIFU-treated and native tissues at 720 and 845 nm laser illuminations. Compared to native tissues, HIFU-induced thermal lesions produced a more than 3-fold enhancement in the PA peak-to-peak signal amplitudes at 720 and 845 nm. This finding indicates that HIFU-induced thermal lesions are indeed detectable with the PA method. It is important to note that HIFU-induced thermal lesions have a higher acoustic attenuation coefficient than native tissues.[1, 2] Therefore, laser-generated PA pressure waves should undergo a greater acoustic attenuation as they propagate through a thermal lesion than native tissue. In fact, the effect of the increased acoustic attenuation is expected to be more pronounced in the PA detection geometry of Fig. 3 (chapter 2), for which the laser source aperture and the ultrasound transducer are on opposite ends of the sample. Nevertheless, in this study, the detected PA signals from HIFU-induced thermal lesions had greater peak-to-peak amplitudes than native tissues, attesting to the high sensitivity of the PA method in detecting HIFU treatments.

The observed PA contrast between HIFU-induced thermal lesions and native tissues may be explained based on Eq. (1-2). While investigating the thermo-acoustic efficiency of HIFU-induced thermal lesions is beyond the scope of this work, the optical properties of these lesions were characterized and compared with native tissues in order to understand the observed PA contrast between HIFU-treated and native tissues. The determination of the optical properties was carried out in the wavelength range of 500-900 nm using a spectrophotometer with an

integrating-sphere attachment. Using the IAD method, the spectrophotometrically-acquired data (TT and DT) were used to determine the optical absorption coefficient and the reduced scattering coefficient of HIFU-treated and native chicken breast tissues in the wavelength range of 500-900 nm. The effective attenuation coefficient and the light penetration depth of HIFU-treated and native chicken breast tissues were calculated in the aforementioned wavelength range using the optical absorption and reduced scattering coefficients. The results quantitatively show the difference between HIFU-treated and native tissues in terms of their DR, DT, μ_a, μ_s', μ_{eff} and D_{eff} in the wavelength range of 500-900 nm. An appropriate range for optical detection of HIFU-treated and native tissues may be extracted from the DR and DT spectra, and then confirmed with the μ_a, μ_{eff}, and D_{eff} spectra. For the tissue model studied, it was found that the wavelength range of 630-900 nm provides the most transmittance and least reflectance, within the wavelength range examined in this study, for HIFU-treated and native tissues. Moreover, the gradual decrease in the effective optical attenuation coefficient and the increase in the effective light penetration depth in the wavelength range of 630-900 nm attest to the previous statement about this range being appropriate for *in vitro* optical detection of HIFU-treated and native chicken breast tissues. Additionally, within the aforementioned wavelength range, the optical absorption coefficient is minimal compared to the surrounding regions, making this range appropriate for optical imaging of relatively deep-seated ROIs. The imaging depth, which is wavelength-dependent, can be inferred from the effective light penetration depth graph (Fig. 12 (b), chapter 2).

The PA contrast between HIFU-induced thermal lesions and native tissues can be attributed, in part, to the HIFU-induced alterations in the molecular and structural composition of the coagulated regions. Protein coagulation, dehydration/tissue shrinkage, and, to less extent, the

formation of methemoglobin are among the mechanisms that may result in changes in the optical properties of thermally-treated tissues *in vitro*, as discussed previously in section III.B.2 (chapter 2). These changes are manifested in the results of the optical spectroscopy experiments, which showed an increase in the optical absorption and reduced scattering coefficients of HIFU-treated tissues. The increase in the optical absorption coefficient results in an increase in the absorbed optical energy (i.e. the product of laser energy fluence and optical absorption coefficient) in Eq. (1-2), thereby enhancing the detected PA pressure (a direct enhancement factor). On the other hand, the increase in the reduced scattering coefficient results in an increase in the effective attenuation coefficient and a decrease in the light penetration depth, increasing the absorbed optical energy, which, in turn, results in an enhancement in the detected PA pressure (an indirect enhancement factor).

3.2 Conclusions

In conclusion, the PA method is capable of detecting HIFU-induced thermal lesions and their associated alterations in the molecular and structural compositions of biologic tissues. The demonstrated, HIFU-induced increase in the peak-to-peak PA signal amplitudes of more than 3 folds at 720 and 845 nm provides experimental evidence to this conclusion.

Based on Eq. (1-2), the results of the spectroscopic investigation can lead to the conclusion that the PA contrast between HIFU-treated and native tissues is due, in part, to direct and indirect optical factors that together contributed to the observed enhancement in the PA pressure detected from HIFU-induced thermal lesions, compared to that detected from native tissues. The direct optical factor is the increase in optical absorption coefficient, increasing the

absorbed optical energy, which is directly proportional to the detected PA pressure (Eq. (1-2)). The indirect optical factor is the large increase in the reduced scattering coefficient, resulting in an increase in the effective optical attenuation coefficient and a decrease in the light penetration depth, which, in turn, increase the absorbed optical energy. The increase in the reduced scattering coefficient can, therefore, indirectly enhance the detected PA pressure by increasing the absorbed optical energy. On the other hand, it is concluded that the effect of the HIFU-induced changes in the acoustic properties of tissue, including the large increase in the acoustic attenuation coefficient of thermal lesions compared to native tissues,[1, 2] on the detected PA pressure is less pronounced than the HIFU-induced changes in the optical properties. This is because the measured changes in the optical properties of HIFU-treated tissues resulted in an enhancement in the detected peak-to-peak PA signal amplitudes, whereas the increased acoustic attenuation coefficient of thermal lesions, determined previously,[1, 2] did not significantly influence the detected PA pressure through the suppression of the peak-to-peak PA signal amplitudes of HIFU-treated tissues.

3.3 Future work

Although the optical properties of HIFU-induced thermal lesions were examined in this study and related to the observed PA contrast between HIFU-induced thermal lesions and native tissues, future work should assess the effects of thermo-acoustic efficiency (Grüneisen parameter) of HIFU-induced thermal lesions on the detected PA pressure rise in a suitable tissue model, such as chicken breast tissue, *in vitro*. Knowledge about the thermo-acoustic efficiency of the examined tissue can expand our understanding with regards to the contribution of each one of the parameters in Eq. (1-2) on the detected PA pressure rise.

Additionally, future work should aim at expanding the current *in vitro* work to a more clinically-relevant scenario (e.g. through the introduction of blood flow in the examined tissue model). It is recommended that the transition from *in vitro* to *in vivo* is done gradually, starting with a freshly-excised *ex vivo* tissue model, an *in vitro* tissue model with a blood flow (such as the one introduced by Arefiev et al.[3]), and then an *in vivo* animal model. The introduction of blood flow will play an important role by influencing the generated PA signals, as discussed in Chapter 2. Moreover, it is recommended that this work is extended to a real-time monitoring of HIFU-induced thermal lesion formation with PA imaging. In this case, although the laser irradiation of PA imaging applied to a ROI prior to HIFU treatments enhances the HIFU-induced heating and temperature rise,[4] there is a need to quantify the HIFU-induced thermal damage following PA imaging. Furthermore, it would be beneficial to observe the PA response from HIFU-induced thermal lesions produced at varying acoustic doses. Last but not least, to enhance the PA detectability of ROIs (e.g. thermal lesions and native tissues), it is suggested to develop a system where multiple diagnostic ultrasound transducers are utilized and placed in front of the sample (i.e. in the laser beam side) as well as behind the sample. Among other advantages, such a modification could potentially enhance the acoustic sensitivity of the PA imaging system.

Chapter 3 bibliography

[1] N. Bush, I. Rivens, G. ter Haar, and J. Bamber, "Acoustic properties of lesions generated with an ultrasound therapy system," Ultrasound in Medicine & Biology **19**, 789–801 (1993).

[2] S. Rahimian and J. Tavakkoli, "Estimating dynamic changes of tissue attenuation coefficient during high-intensity focused ultrasound treatment," Journal of Therapeutic Ultrasound **14**, 1–22 (2013).

[3] A. Arefiev, F. Prat, J. Chapelon, J. Tavakkoli, and D. Cathignol, "Ultrasound-induced tissue ablation: studies on isolated, perfused porcine liver," Ultrasound in Medicine & Biology **24**, 1033–1043 (1998).

[4] H. Cui and X. Yang, "Enhanced-heating effect during photoacoustic imaging-guided high-intensity focused ultrasound," Applied Physics Letters **99**, 231113 (2011).

Appendix A: Linear acoustic intensity simulation - parameters and results

Utilizing a linear acoustic and temperature simulation (LATS),[1, 2] 1-D and 2-D acoustic intensity profiles were calculated for the HIFU transducer used in this study, with a simulated geometry shown in Fig. A-1. The simulation was run once with free-field acoustic parameters and once with adjusted acoustic parameters that accounted for the presence of chicken breast tissue in the medium of propagation.

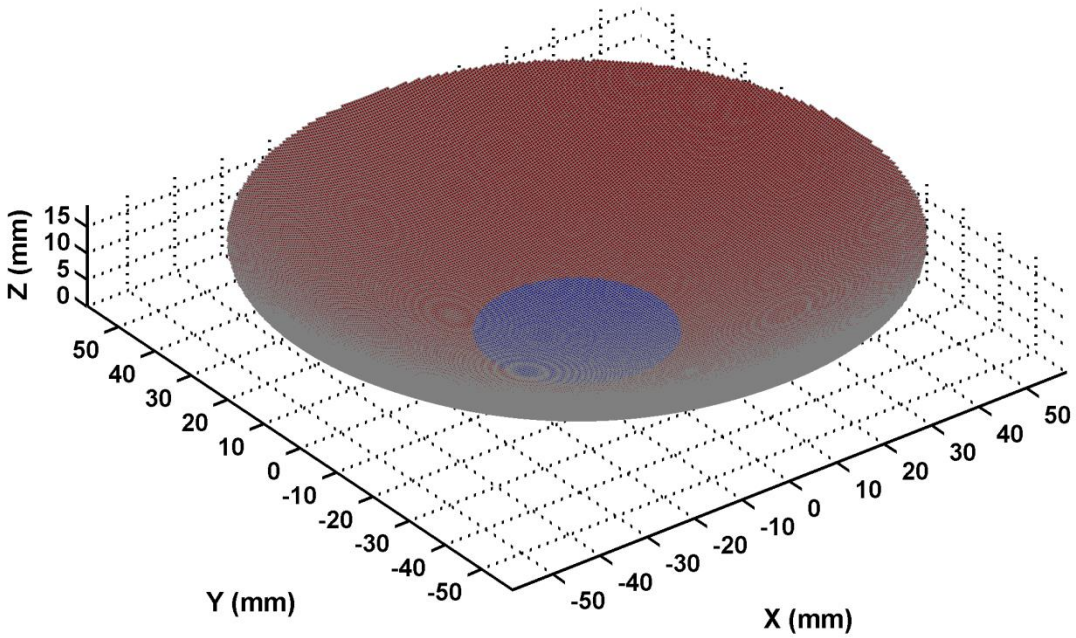

FIG. A-1: Simulated geometry of the HIFU transducer used in this study. The blue circle, made to accommodate a confocal imaging probe, is a 35-mm-diameter hole that has been excluded from the acoustic field calculations.

Free-field simulation parameters and results

Table A-1 contains the acoustic parameters of pure water at 20 ^{o}C that were used in the simulation program as medium properties, in addition to other parameters related to transducer properties/features and the calculation volume, as shown in Fig. A-2.

Table A-1: The acoustic properties of pure water at 20 ^{o}C (obtained from Ref.[3])

Speed of sound	1482.34 m/s
Density	998.2 kg/m^3
Acoustic attenuation coefficient	0.0022 dB/(cm·MHz^2)
Attenuation frequency dependency (n)	2

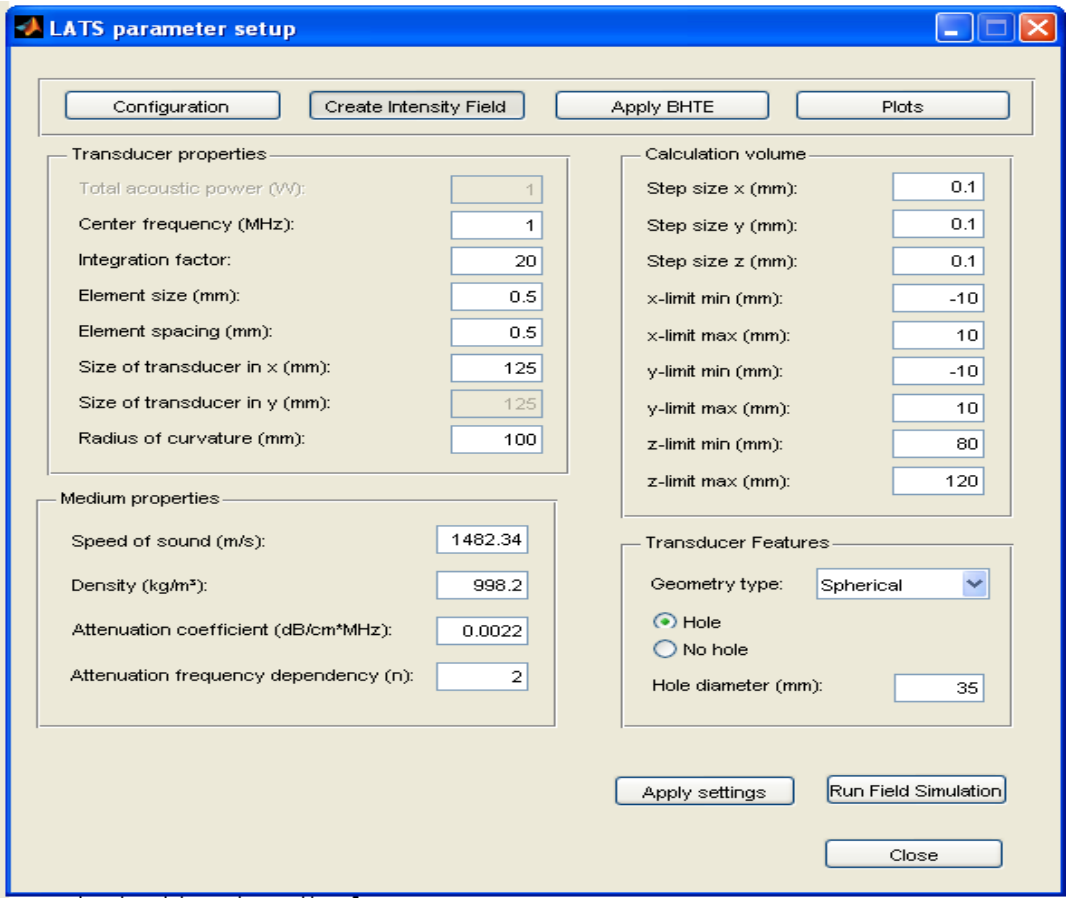

FIG.A-1: A snapshot of the LATS parameters setup window for the free-field simulation.

The results of the free-field simulation are shown in Fig. A-3 for the 1-D and 2-D axial as well as lateral intensity profiles of the HIFU regime employed in this study.

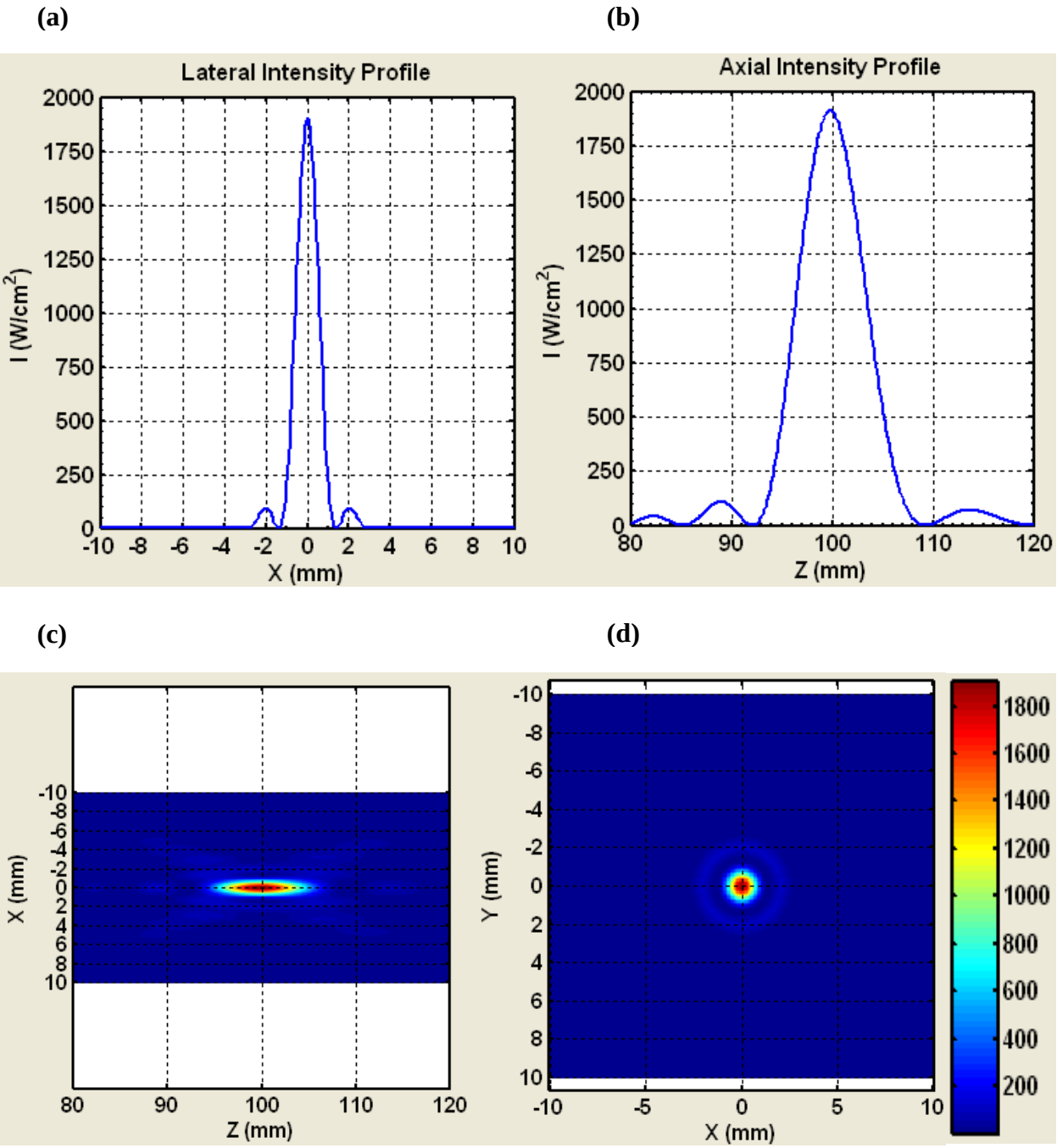

FIG. A-3: Results of the free-field simulation showing the 1-D (a) lateral and (b) axial as well as the 2-D (c) axial and (d) lateral intensity profiles. The free-field focal intensity I_{SPTA} is calculated as approximately 1910 W/cm^2.

Water-tissue adjusted simulation parameters and results

The acoustic properties of chicken breast tissues (Table A-2) were adjusted with the pure water acoustic properties (Table A-1) in order to obtain corrected values for the medium properties, taking into account the ultrasound propagation distances in water (~9.0 cm) and in tissue (~1.0 cm), as per Eq. (A-1). The adjusted medium acoustic parameters were inputted in the simulation program, in addition to other parameters related to transducer properties/features and the calculation volume, as shown in Fig. A-4.

Table A-2: The acoustic properties of chicken breast tissue (obtained from Ref. [4])

Speed of sound	1585 m/s
Density	1040 kg/m^3
Acoustic attenuation coefficient	0.4343 dB/(cm·MHz$^{1.1}$)
Attenuation frequency dependency (n)	1.1

The formula used to apply tissue parameters adjustment is:

$$C = \frac{L_T}{F_L} \cdot A + \frac{L_W}{F_L} \cdot B \qquad \text{(A-1)}$$

where C represents the corrected acoustic property, A is the tissue acoustic property, B is the water acoustic property, L_T is the tissue focal depth (i.e. distance of ultrasound propagation in tissue, which was approximately 1.0 cm in this study), L_W is the distance of ultrasound propagation in water (~9.0 cm in this study), and F_L denotes the focal length of the HIFU transducer (~10.0 cm).

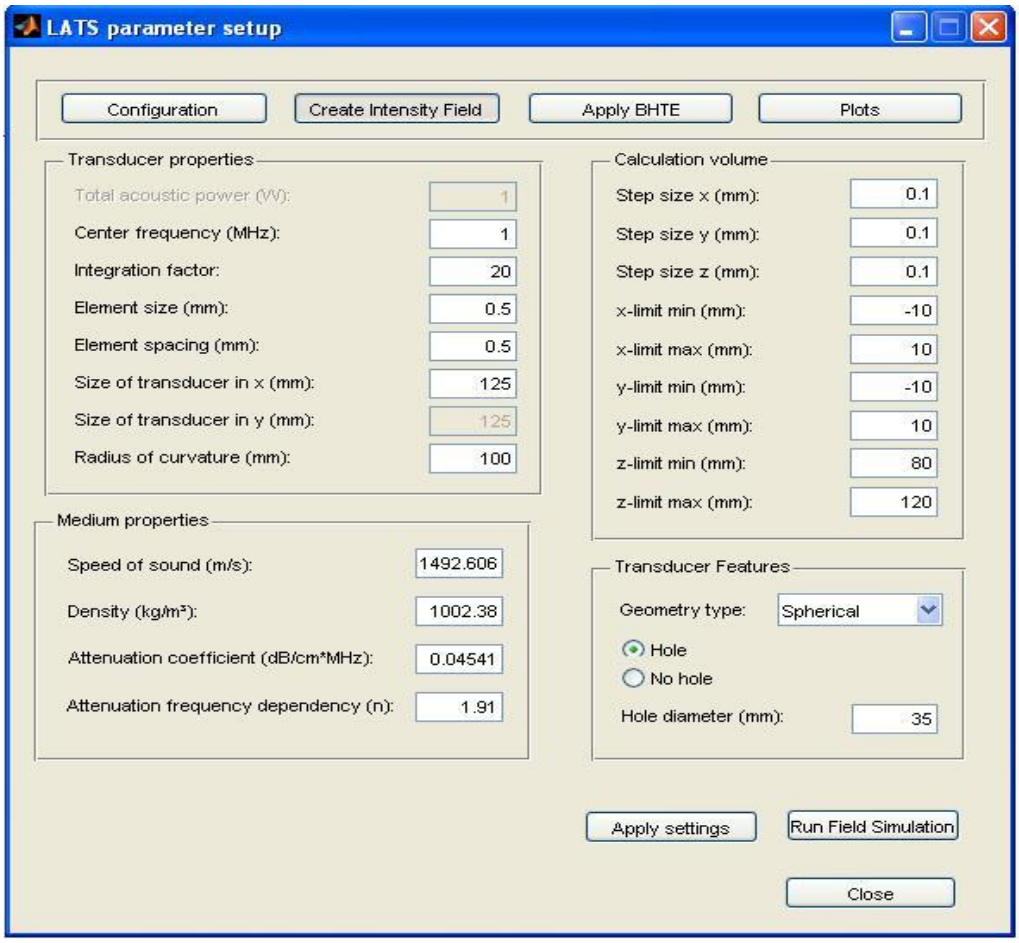

FIG. A-4: A snapshot of the LATS parameter setup window for the water-tissue adjusted simulation.

The results of the water-tissue adjusted simulation are shown in Fig. A-5 for the 1-D and 2-D axial as well as lateral intensity profiles of the HIFU treatment regime employed in this study. These results were used to obtain an estimate of the focal intensity (I_{SPTA}) achieved during HIFU treatments. Moreover, the intensity profiles of the HIFU treatments were used to obtain: **(a)** the location of the maximum focal intensity (~10 cm); **(b)** the -6 dB HIFU beam width at the focus (~1.24 mm) from the lateral intensity profiles, Fig. A-5 (a and d) and **(c)** the depth of field of the HIFU beam (~7.55 mm) from the axial intensity profiles, Fig. A-5 (b and c).

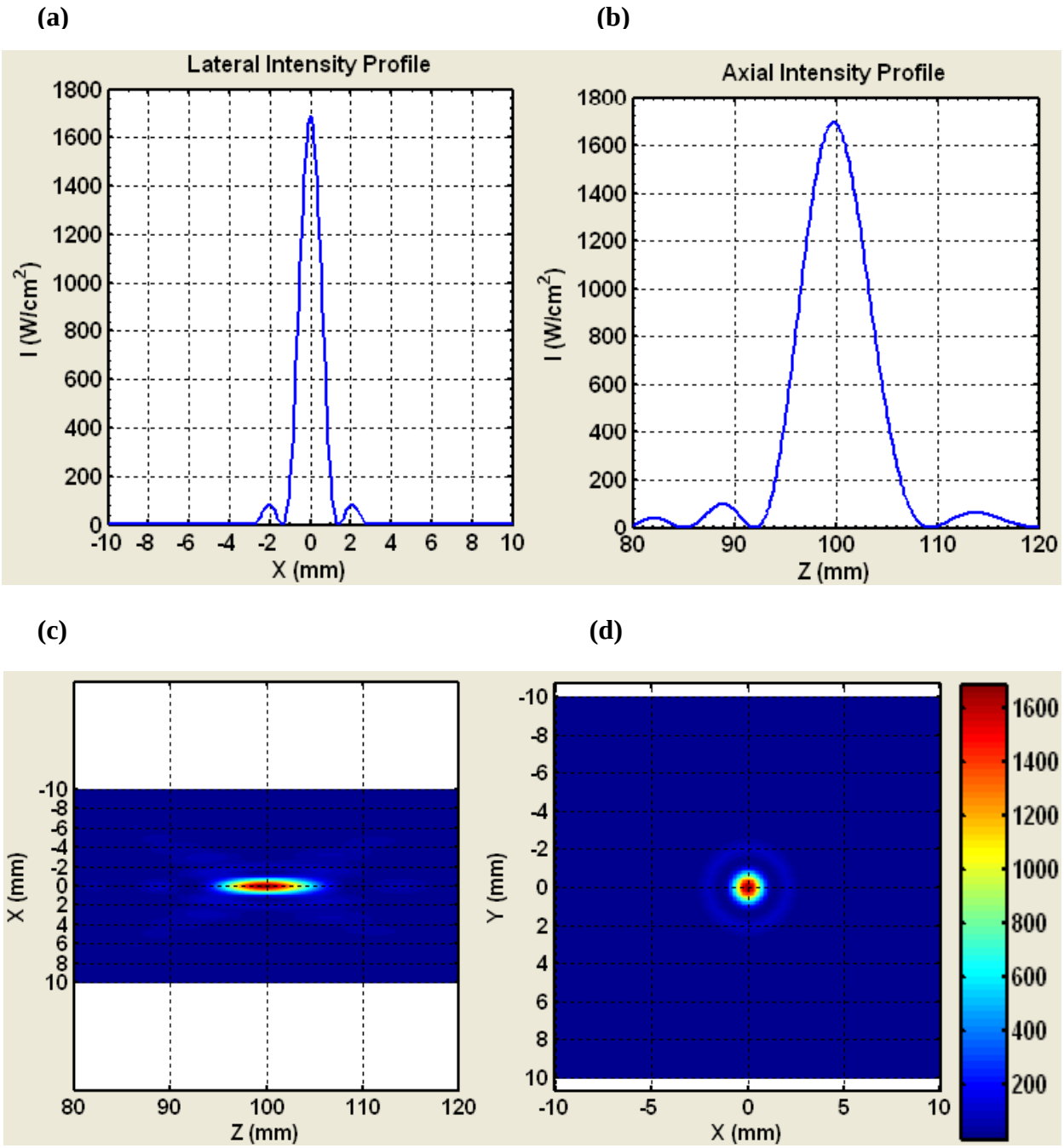

FIG.A-5: Results of the water-tissue adjusted simulation showing the 1-D (a) lateral and (b) axial intensity profiles as well as the 2-D (c) axial and (d) lateral intensity profiles. The focal intensity I_{SPTA} is approximately 1690 W/cm^2.

Appendix B: The inverse adding-doubling method

In conjunction with spectroscopic measurements, the inverse adding-doubling (IAD) method[5] was used in this study to determine the optical properties of HIFU-treated chicken breast tissues. In the IAD program,[6] optical parameters such as scattering, absorption, and scattering anisotropy can be determined by repeatedly solving the radiative transport equation (RTE) until a match with the measured reflection and transmission values is determined.[5] The RTE, which describes the behaviour of light in a medium that absorbs, scatters and emits radiation, is given by the following mathematical expression[7, 8]:

$$(\hat{\boldsymbol{s}} \cdot \nabla) L(\boldsymbol{r}, \hat{\boldsymbol{s}}) = -\mu_t L(\boldsymbol{r}, \hat{\boldsymbol{s}}) + \mu_{\boldsymbol{s}} \int_{4\pi} p(\hat{\boldsymbol{s}}, \hat{\boldsymbol{s}'}) L(\boldsymbol{r}, \hat{\boldsymbol{s}})\, dw' \tag{B-2}$$

where $L(\boldsymbol{r}, \hat{\boldsymbol{s}})$ is the radiance, also known as specific intensity, in units of energy per area per solid angle in the position denoted by the vector $\boldsymbol{r}$ and in the direction specified by the unit vector $\hat{\boldsymbol{s}}$.[8] The total attenuation μ_t is the sum of the absorption coefficient μ_a and the scattering coefficient $\mu_{\boldsymbol{s}}$, i.e. it is given by the following mathematical expression[8]:

$$\mu_t = \mu_a + \mu_{\boldsymbol{s}} \tag{B-3}$$

In Eq. (B-2), the phase function $p(\hat{\boldsymbol{s}}, \hat{\boldsymbol{s}'})$ denotes the fraction of light that is scattered in the direction of the unit vector $\hat{\boldsymbol{s}'}$ as a result of an incident light from the direction of $\hat{\boldsymbol{s}}$, and dw' is the differential solid angle in the direction of $\hat{\boldsymbol{s}'}$.[8] The left hand side of Eq. (B-2) describes the rate of change of the radiance at the point $\boldsymbol{r}$ and in the direction $\hat{\boldsymbol{s}}$.[8] This rate of change of the radiance is equal to the radiance lost as a result of absorption and scattering, which the first term on the right hand side, in addition to the radiance gained as a result of light being scattered from all other directions into the direction of the unit vector $\hat{\boldsymbol{s}}$, which is the second term on the right hand side.[8]

In the IAD method, the "inverse" implies a reversal to the regular extraction of transmission and reflection values from the optical properties, whereas "adding-doubling" refers to the utilized methodology in solving the RTE.[5] The IAD method, therefore, converts the integrating-sphere measurements of diffuse reflectance and total transmittance into optical absorption and reduced scattering coefficients.[9] It is a versatile method, and is well-suited to measurements employing biologic tissue specimens positioned between optical glass slides/plates.[5] Figure B-6 shows a flow chart of the method.

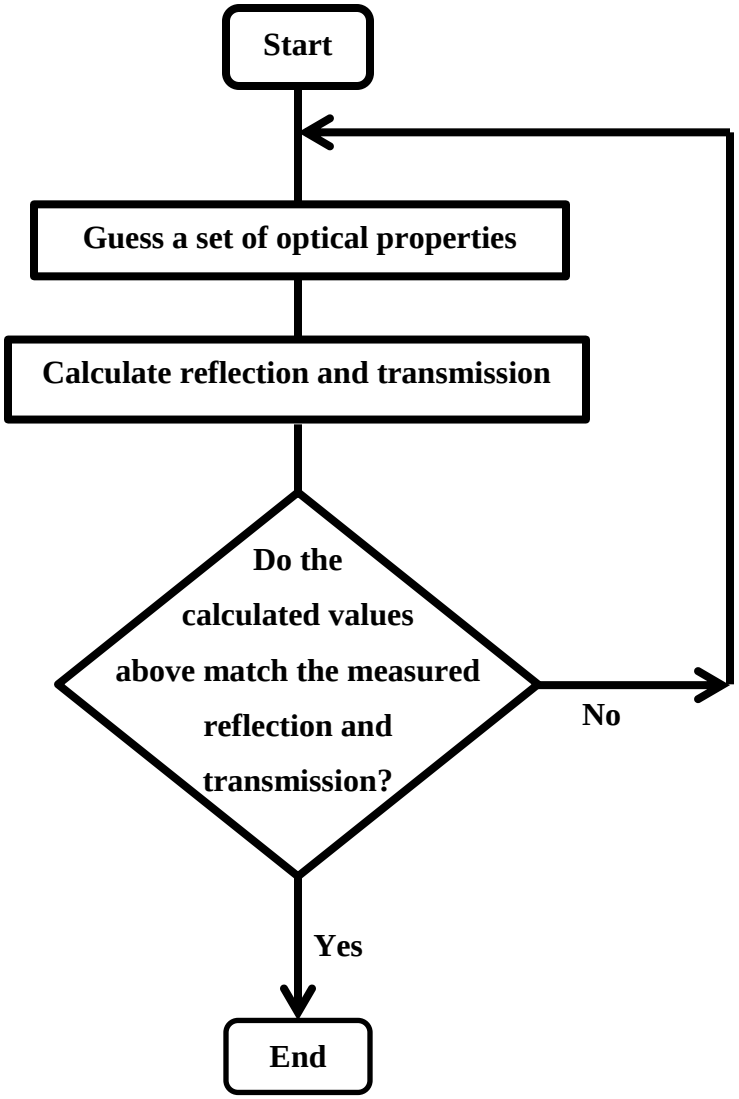

FIG. B-6: Flow chart of the IAD method (reproduced, with permission, from Dr. S. A. Prahl's PhD dissertation[8]).

Table B-3 summarizes the parameters that were inputted into the IAD program in order to obtain the optical properties from the diffuse reflectance and total transmittance measurements on chicken breast slices sandwiched between two BK-7 optical glass slides.

Table B-3: Parameters used in the IAD program

Index of refraction of the sample **(chicken breast tissue)**	1.37 (Ref. [10])
Index of refraction of the top and bottom slides **(BK-7)**	1.51 (Ref. [11])
Thickness of sample	1.0 mm
Thickness of slides	1.0 mm
Diameter of illumination beam	7.14 mm
Reflectivity of the reflectance calibration standard	0.98
Number of spheres used during each measurement	1
Properties of reflectance measurement sphere	
Sphere diameter	*60 mm*
Sample port diameter	*18.75 mm*
Entrance port diameter	*16.74 mm*
Detector port diameter	*13.12 mm*
Reflectivity of the sphere wall	*0.98*
Properties of transmittance measurement sphere	
Sphere diameter	*60 mm*
Sample Port Diameter	*16.74 mm*
Entrance Port Diameter	*0.00 mm*
Detector Port Diameter	*13.12 mm*
Reflectivity of the sphere wall	*0.98*
Number of measurements: M_R M_T	2

Appendices bibliography

[1] F. Butt, A. Abhari, and J. Tavakkoli, "An application of high performance computing to improve linear acoustic simulation," Proceedings of the 2011 Spring Simulation Multi-conference 71–78 (2011).

[2] F. Butt, High performance computing for linear acoustic wave simulation (Ryerson University, 2011).

[3] R. Cobbold, *Foundations of Biomedical Ultrasound* (Oxford University Press, New York, NY, 2007).

[4] M.T. Adams, Q. Wang, R.O. Cleveland, and R.A. Roy, "Improving the acousto-optic detection of high-intensity focused ultrasound lesions," Proceedings of Meetings on Acoustics **19**, 075065 (2013).

[5] S.A. Prahl, M.J.C. van Gemert, and A.J. Welch, "Determining the optical properties of turbid media by using the adding-doubling method," Applied Optics **32**, 559–568 (1993).

[6] S.A. Prahl, *Inverse Adding-Doubling program: Version 3-9-6*, (2013). (http://omlc.ogi.edu/software/iad/index.html)

[7] S. Chandrasekhar, *Radiative Transfer* (Dover Publications Inc., New York, 1960).

[8] S.A. Prahl, Light Transport in Tissue (The University of Texas at Austin, 1988).

[9] S. Prahl, "Everything I think you should know about inverse adding-doubling," Oregon Medical Laser Center, St. Vincent Hospital 1–74 (2011).

[10] G. Marquez, L. V Wang, S.P. Lin, J.A. Schwartz, and S.L. Thomsen, "Anisotropy in the absorption and scattering spectra of chicken breast tissue," Applied Optics **37**, 798–804 (1998).

[11] Esco Optics Inc., *Material Data- BK7 Optical Glass*, (2012).